

Advanced Concepts for Adaptive Optics Compensation for Imaging and Propagation through Strong Turbulence

Glenn A. Tyler

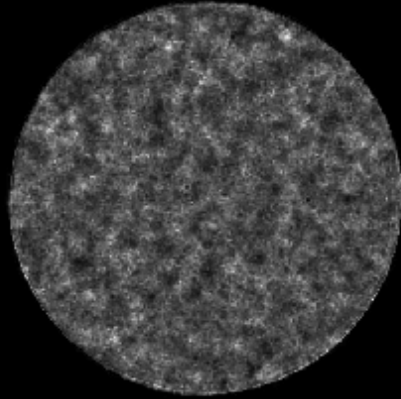
8 August 2005

Introduction

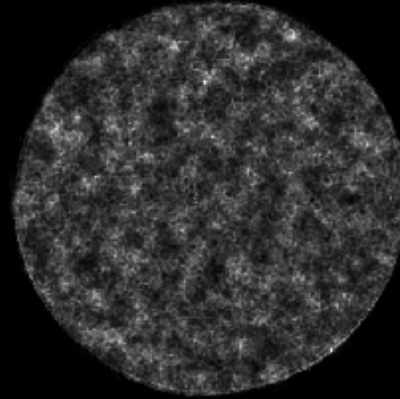
- Recent advances in wavefront reconstructor technology and MCAO techniques support adaptive optics transmission through strong turbulence
- This work will summarize the following advances
 - Branch Cut Reconstructors
 - MCAO field conjugation
 - Gradient Descent Tomography
- Applications involve
 - Low elevation astronomy
 - Laser communications
 - Power beaming
 - Isoplanatic imaging
- Work supported by the Optical Sciences Company under Internal Research and Development

Sample Pupil Plane Intensity: Low Elevation Propagation for Power beaming or Astronomy

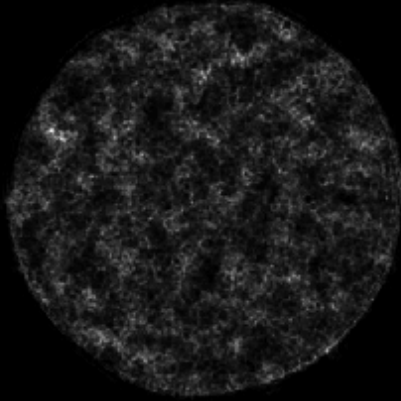
0°



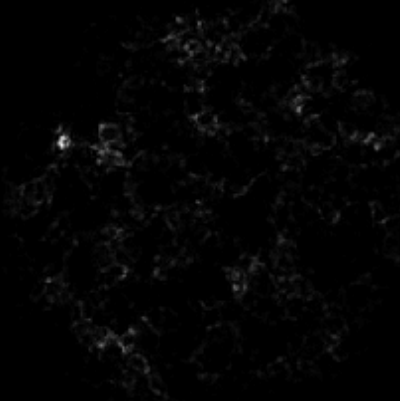
45°



60°

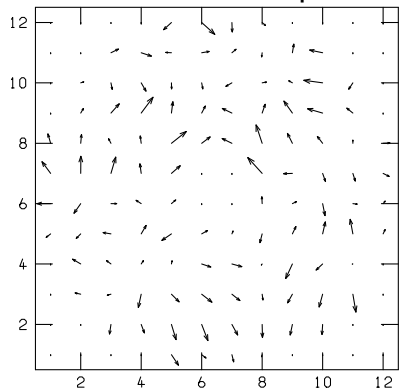


80°

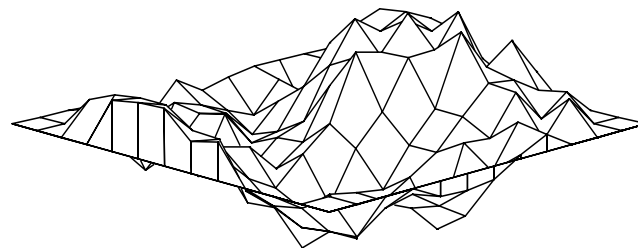


The Concept of Slope Discrepancy

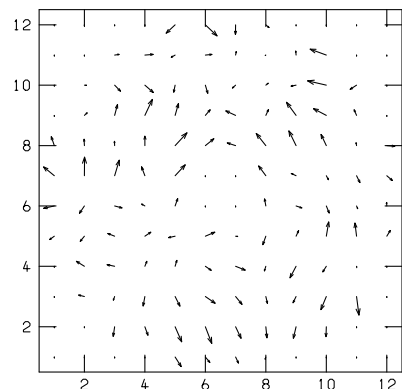
Measured Slopes



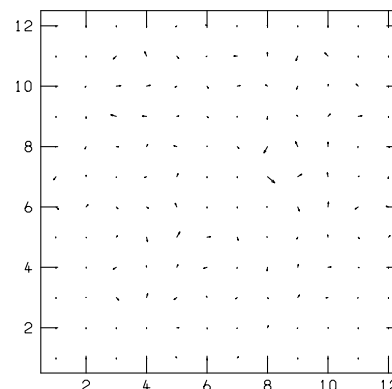
Reconstructed Wavefront



Slopes From Reconstructed Wavefront



Slope Discrepancy (Noise)



- The Slope Discrepancy is found by numerically differentiating the reconstructed wavefront and comparing the computed slopes with the originally measured slopes
- The slopes consistent with reconstructed wavefront distortion are given by: $s = \Gamma p = \Gamma(\Gamma^T \Gamma)^{-1} \Gamma^T s_0$, $p = (\Gamma^T \Gamma)^{-1} \Gamma^T s_0$
- The Slope Discrepancy is then: $s_0 - s = [I - \Gamma(\Gamma^T \Gamma)^{-1} \Gamma^T] s_0$
- When noise is present the Slope Discrepancy is not zero
- We find that about half of the noise is reconstructible
- This occurs because the component of the gradient field with a CURL not equal to zero is not reconstructible with a Least Square reconstructor

Rigorous Decomposition of a General Vector Field

- The analysis begins with the well known vector identity

$$\nabla \cdot \nabla A(\mathbf{r}, z) = \nabla[\nabla \cdot A(\mathbf{r}, z)] - \nabla \times \nabla \times A(\mathbf{r}, z)$$

- Fourier analysis is used to simplify this result

$$A(\mathbf{r}, z) = \int d\alpha \tilde{A}(\boldsymbol{\kappa}, s) \exp[2\pi i(\boldsymbol{\alpha} \cdot \mathbf{x})], \quad \tilde{A}(\boldsymbol{\kappa}, s) = \int d\mathbf{x} A(\mathbf{r}, z) \exp[-2\pi i(\boldsymbol{\alpha} \cdot \mathbf{x})]; \quad \mathbf{x} = (\mathbf{r}, z), \quad \boldsymbol{\alpha} = (\boldsymbol{\kappa}, s)$$

- The vector identity becomes

$$-4\pi\boldsymbol{\alpha} \cdot \boldsymbol{\alpha} \tilde{A}(\boldsymbol{\alpha}) = -4\pi\boldsymbol{\alpha} \boldsymbol{\alpha} \cdot \tilde{A}(\boldsymbol{\alpha}) + 4\pi\boldsymbol{\alpha} \times \boldsymbol{\alpha} \times \tilde{A}(\boldsymbol{\alpha})$$

- In Fourier space the solution is

$$\tilde{A}(\boldsymbol{\alpha}) = 2\pi i \boldsymbol{\alpha} \frac{\boldsymbol{\alpha} \cdot \tilde{A}(\boldsymbol{\alpha})}{2\pi \alpha^2} - 2\pi i \boldsymbol{\alpha} \times \frac{\boldsymbol{\alpha} \times \tilde{A}(\boldsymbol{\alpha})}{2\pi \alpha^2}$$

- The application of an inverse Fourier transform results in the desired expression

$$A(\mathbf{x}) = \nabla \varphi(\mathbf{x}) + \nabla \times V(\mathbf{x}); \quad \varphi(\mathbf{x}) = \int d\boldsymbol{\alpha} \frac{\boldsymbol{\alpha} \cdot \tilde{A}(\boldsymbol{\alpha})}{2\pi \alpha^2} \exp[2\pi i(\boldsymbol{\alpha} \cdot \mathbf{x})], \quad V(\mathbf{x}) = \int d\boldsymbol{\alpha} \frac{\boldsymbol{\alpha} \times \tilde{A}(\boldsymbol{\alpha})}{-2\pi \alpha^2} \exp[2\pi i(\boldsymbol{\alpha} \cdot \mathbf{x})]$$

- A key feature of this approach is the fact that the scalar and vector potentials are expressed in terms of the Fourier transform of the vector field of interest (We have “reconstructed” the scalar and vector potentials from the data.)

Application of the Fourier Decomposition Technique to the Wavefront Gradient Field

- For the two dimensional wavefront gradient field we have

$$A(\mathbf{x}) = g_x(\mathbf{r})\mathbf{u}_x + g_y(\mathbf{r})\mathbf{u}_y \quad \text{and} \quad \tilde{A}(\boldsymbol{\alpha}) = \tilde{g}_x(\boldsymbol{\kappa})\delta(s)\mathbf{u}_x + \tilde{g}_y(\boldsymbol{\kappa})\delta(s)\mathbf{u}_y; \quad \mathbf{x} = (\mathbf{r}, z), \quad \boldsymbol{\alpha} = (\boldsymbol{\kappa}, s)$$

- In terms of the scalar and vector potentials, the wavefront gradient field is given by

$$\mathbf{g}(\mathbf{r}) = \nabla_{\perp}\varphi(\mathbf{r}) + \nabla \times \mathbf{u}_z V(\mathbf{r}); \quad \varphi(\mathbf{r}) = \int d\boldsymbol{\kappa} \frac{\kappa_x \tilde{g}_x(\boldsymbol{\kappa}) + \kappa_y \tilde{g}_y(\boldsymbol{\kappa})}{2\pi i \kappa^2} \exp(2\pi i \boldsymbol{\kappa} \cdot \mathbf{r}), \quad V(\mathbf{r}) = \int d\boldsymbol{\kappa} \frac{\kappa_y \tilde{g}_x(\boldsymbol{\kappa}) - \kappa_x \tilde{g}_y(\boldsymbol{\kappa})}{-2\pi i \kappa^2} \exp(2\pi i \boldsymbol{\kappa} \cdot \mathbf{r}), \quad V(\mathbf{r}) = \mathbf{u}_z V(\mathbf{r})$$

- As a consequence the gradient field can be decomposed into two components, LS for least square and SD for slope discrepancy

$$\mathbf{g}(\mathbf{r}) = \mathbf{g}_{LS}(\mathbf{r}) + \mathbf{g}_{SD}(\mathbf{r}); \quad \mathbf{g}_{LS}(\mathbf{r}) = \nabla_{\perp}\varphi(\mathbf{r}), \quad \mathbf{g}_{SD}(\mathbf{r}) = \nabla \times \mathbf{u}_z V(\mathbf{r})$$

- The phase is decomposed in the same way

$$\varphi_{Total}(\mathbf{r}) = \varphi_{LS}(\mathbf{r}) + \varphi_{SD}(\mathbf{r}); \quad \nabla \varphi_{Total}(\mathbf{r}) = \mathbf{g}(\mathbf{r}), \quad \nabla \varphi_{LS}(\mathbf{r}) = \mathbf{g}_{LS}(\mathbf{r}), \quad \nabla \varphi_{SD}(\mathbf{r}) = \mathbf{g}_{SD}(\mathbf{r})$$

- Both components of the phase are reconstructed by integrating the following set of equations

$$\text{For LS: } \frac{\partial}{\partial x} \varphi_{LS}(\mathbf{r}) = \frac{\partial}{\partial x} \varphi(\mathbf{r}) \text{ and } \frac{\partial}{\partial y} \varphi_{LS}(\mathbf{r}) = \frac{\partial}{\partial y} \varphi(\mathbf{r})$$

$$\text{For SD: } \frac{\partial}{\partial x} \varphi_{SD}(\mathbf{r}) = \frac{\partial}{\partial y} V(\mathbf{r}) \text{ and } \frac{\partial}{\partial y} \varphi_{SD}(\mathbf{r}) = -\frac{\partial}{\partial x} V(\mathbf{r})$$

- As a consequence, the LS phase is equal to the scalar potential and the SD phase is the imaginary part of the analytic function whose real part is minus the vector potential
- A key feature of the Fourier approach is the fact that the locations of the branch points need not be known. All the information is contained the gradient field.

Relation to Other Work

- Discrete Least Square reconstruction^{1,2}

- The discrete form of the required operators can be expressed in terms of the Gamma matrix

$$\textit{Gradient} : \nabla \Rightarrow \Gamma, \quad \textit{Divergence} : \nabla \cdot \Rightarrow \Gamma^T, \quad \textit{Laplacian} : \nabla \cdot \nabla \Rightarrow \Gamma^T \Gamma$$

- In discrete form the potentials and the gradient field components are given by

$$\phi = (\Gamma^T \Gamma)^{-1} \Gamma^T \mathbf{g}, \quad V = (\Gamma^T \Gamma)^{-1} C_z \mathbf{g}, \quad \mathbf{g}_{LS} = \Gamma (\Gamma^T \Gamma)^{-1} \Gamma^T \mathbf{g}, \quad \mathbf{g}_{SD} = C_{xy} (\Gamma^T \Gamma)^{-1} C_z \mathbf{g}, \quad \textit{where } C_{xy} \textit{ and } C_z \textit{ are Curl operators}$$

- As a consequence the new theory illustrates that the slope discrepancy gradient field is given by the well known expression which represents the Curl of the Vector Potential⁴

$$\mathbf{g}_{SD} = \mathbf{g} - \mathbf{g}_{LS} = \left[I - \Gamma (\Gamma^T \Gamma)^{-1} \Gamma^T \right] \mathbf{g}$$

- Branch Point contribution to the phase

- As reported in the literature many researchers are investigating the contribution of branch points in the phase function and are pursuing a path that requires the location of each branch point to be known³
- In terms of Reference 3 our vector potential, V, is equal to the Hertz potential, h, and our slope discrepancy phase, ϕ_{SD} , is identical to the hidden phase, ϕ_{hid} .

- It is important to note that this new formulation of the problem does not require the location of the Branch Points and works with the gradient field directly. In addition we avoid the use of the term hidden phase since it is readily available.

1. D. M. Winker, G. A. Ameer, S. L. Browne, G. C. Cochran, R. H. Dueck, D. L. Fried, D. M. Lussier, W. Moretti, P. H. Roberts, K. E. Steinhoff and G. A. Tyler, "Characteristics of Turbulence Measured on a Large Aperture," SPIE Vol. **926**, 360-366 (1988).
2. William Moretti, Gregory M. Cochran, Karl E Steinhoff and Glenn A. Tyler, "SOR-3 Data Reduction," Report Number TR-881, the Optical Sciences Company, Anaheim CA (1988)
3. David L. Fried, "Branch Point Problem in Adaptive Optics," JOSA A **15**, 2759-2768 (1998).
4. Glenn A. Tyler, "Reconstruction and Assessment of the Least-Squares and Slope Discrepancy Components of the Phase," JOSA A **17** 1828-1839 (2000)

An Analytic Example

- It is instructive to consider the phase (which has a single branch point at $z=0$) associated with the complex function $z=x+iy$:

$$\phi_{Total}(\mathbf{r}) = \tan^{-1}\left(\frac{y}{x}\right)$$

- The gradient field is then

$$\mathbf{g}_x(\mathbf{r}) = \frac{\partial}{\partial x} \phi_{Total}(\mathbf{r}) = \frac{-y}{x^2+y^2}, \quad \mathbf{g}_y(\mathbf{r}) = \frac{\partial}{\partial y} \phi_{Total}(\mathbf{r}) = \frac{x}{x^2+y^2}$$

- The Fourier transform of the gradient field is

$$\tilde{\mathbf{g}}_x(\boldsymbol{\kappa}) = \int d\mathbf{r} \frac{-y}{x^2+y^2} \exp(2\pi i \boldsymbol{\kappa} \cdot \mathbf{r}) = i \frac{\kappa_y}{\kappa^2}, \quad \tilde{\mathbf{g}}_y(\boldsymbol{\kappa}) = \int d\mathbf{r} \frac{x}{x^2+y^2} \exp(2\pi i \boldsymbol{\kappa} \cdot \mathbf{r}) = -i \frac{\kappa_x}{\kappa^2}$$

- The potentials are

$$\varphi(\mathbf{r}) = \frac{1}{2\pi i} \int d\boldsymbol{\kappa} \frac{\kappa_x \tilde{\mathbf{g}}_x(\boldsymbol{\kappa}) + \kappa_y \tilde{\mathbf{g}}_y(\boldsymbol{\kappa})}{\kappa^2} \exp(2\pi i \boldsymbol{\kappa} \cdot \mathbf{r}) = 0, \quad V(\mathbf{r}) = \frac{1}{2\pi i} \int d\boldsymbol{\kappa} \frac{\kappa_y \tilde{\mathbf{g}}_x(\boldsymbol{\kappa}) - \kappa_x \tilde{\mathbf{g}}_y(\boldsymbol{\kappa})}{\kappa^2} \exp(2\pi i \boldsymbol{\kappa} \cdot \mathbf{r}) = \frac{1}{2\pi} \int d\boldsymbol{\kappa} \kappa^{-2} \exp(2\pi i \boldsymbol{\kappa} \cdot \mathbf{r})$$

- As a consequence the gradient field components are

$$\mathbf{g}_{LS}(\mathbf{r}) = \nabla \varphi(\mathbf{r}) = 0, \quad \mathbf{g}_{SD}(\mathbf{r}) = \nabla \times \mathbf{u}_z \frac{1}{2\pi} \int d\boldsymbol{\kappa} \kappa^{-2} \exp(2\pi i \boldsymbol{\kappa} \cdot \mathbf{r}) = \frac{-y}{r^2} \mathbf{u}_x + \frac{x}{r^2} \mathbf{u}_y$$

- The phase is found by integration

$$\phi_{Total}(\mathbf{r}) = \phi_{SD}(\mathbf{r}) = \int_0^y dy \frac{x}{x^2+y^2} = \tan^{-1}\left(\frac{y}{x}\right)$$

White Noise is Nearly Equally Distributed Between the Two Components of the Gradient Field

- It is assumed that the total gradient field is due to white noise

$$\mathbf{g} = \mathbf{n}, \quad \langle \mathbf{n}\mathbf{n}^T \rangle = I_{n_s} \sigma_n^2$$

- The two components of the gradient field are

$$\mathbf{g}_{LS} = \Gamma(\Gamma^T \Gamma)^{-1} \Gamma^T \mathbf{n}, \quad \mathbf{g}_{SD} = \left[I_{n_s} - \Gamma(\Gamma^T \Gamma)^{-1} \Gamma^T \right] \mathbf{n}$$

- The Least Square variance is

$$\begin{aligned} \sigma_{LS}^2 &= \frac{1}{n_s} \text{Tr} \langle \mathbf{g}_{LS} \mathbf{g}_{LS}^T \rangle = \frac{1}{n_s} \text{Tr} \left[\Gamma(\Gamma^T \Gamma)^{-1} \Gamma^T \langle \mathbf{n}\mathbf{n}^T \rangle \Gamma(\Gamma^T \Gamma)^{-1} \Gamma^T \right] \\ &= \frac{\sigma_n^2}{n_s} \text{Tr} \left[\Gamma(\Gamma^T \Gamma)^{-1} \Gamma^T \right] = \frac{\sigma_n^2}{n_s} \text{Tr} \left[(\Gamma^T \Gamma)^{-1} \Gamma^T \Gamma \right] = \frac{\sigma_n^2}{n_s} \text{Tr} (I_{n_p-2}) \\ &= \frac{n_p-2}{n_s} \sigma_n^2 \end{aligned}$$

- The Slope Discrepancy variance is

$$\begin{aligned} \sigma_{SD}^2 &= \frac{1}{n_s} \text{Tr} \langle \mathbf{g}_{SD} \mathbf{g}_{SD}^T \rangle = \frac{1}{n_s} \text{Tr} \left\{ \left[I_{n_s} - \Gamma(\Gamma^T \Gamma)^{-1} \Gamma^T \right] \langle \mathbf{n}\mathbf{n}^T \rangle \left[I_{n_s} - \Gamma(\Gamma^T \Gamma)^{-1} \Gamma^T \right] \right\} \\ &= \frac{\sigma_n^2}{n_s} \text{Tr} \left[I_{n_s} - \Gamma(\Gamma^T \Gamma)^{-1} \Gamma^T \right] = \frac{\sigma_n^2}{n_s} \text{Tr} \left[I_{n_s} - (\Gamma^T \Gamma)^{-1} \Gamma^T \Gamma \right] = \frac{\sigma_n^2}{n_s} \text{Tr} (I_{n_s} - I_{n_p-2}) \\ &= \frac{n_s - n_p + 2}{n_s} \sigma_n^2 \end{aligned}$$

- Since there are approximately twice as many gradients as phase points, both components are approximately equal

Fitting Error Contributes to the Slope Discrepancy Gradient Field

- Sensor fitting error occurs because the discrete gradient operator does not perfectly represent the relationship between the measured gradients and the phase
- The Slope Discrepancy Gradient field associated with this error is

$$\begin{aligned}
 \mathbf{g}_{SD} &= \left[I_{n_s} - \Gamma(\Gamma^T \Gamma)^{-1} \Gamma^T \right] \mathbf{n}, \quad \mathbf{n} = \mathbf{g}_s - \Gamma \mathbf{p}, \quad \mathbf{p} = \boldsymbol{\varphi}_{Total} \\
 &= \left[I_{n_s} - \Gamma(\Gamma^T \Gamma)^{-1} \Gamma^T \right] \mathbf{g}_s - \left[I_{n_s} - \Gamma(\Gamma^T \Gamma)^{-1} \Gamma^T \right] \Gamma \mathbf{p} \\
 &= \left[I_{n_s} - \Gamma(\Gamma^T \Gamma)^{-1} \Gamma^T \right] \mathbf{g}_s - \left[\Gamma - \Gamma(\Gamma^T \Gamma)^{-1} \Gamma^T \Gamma \right] \mathbf{p} \\
 &= \left[I_{n_s} - \Gamma(\Gamma^T \Gamma)^{-1} \Gamma^T \right] \mathbf{g}_s
 \end{aligned}$$

- The Slope Discrepancy variance is expressed in terms of the G-Tilt covariance matrix

$$\sigma_{SD}^2 = \frac{1}{n_s} Tr \left\langle \mathbf{g}_{SD} \mathbf{g}_{SD}^T \right\rangle = \frac{1}{n_s} Tr \left[I_{n_s} - \Gamma(\Gamma^T \Gamma)^{-1} \Gamma^T \right] \left\langle \mathbf{g}_s \mathbf{g}_s^T \right\rangle \left[I_{n_s} - \Gamma(\Gamma^T \Gamma)^{-1} \Gamma^T \right]$$

- This can be as large as a few hundred nanoradians for systems of interest

Simulation Results: Initial Wavefront Gradient Field

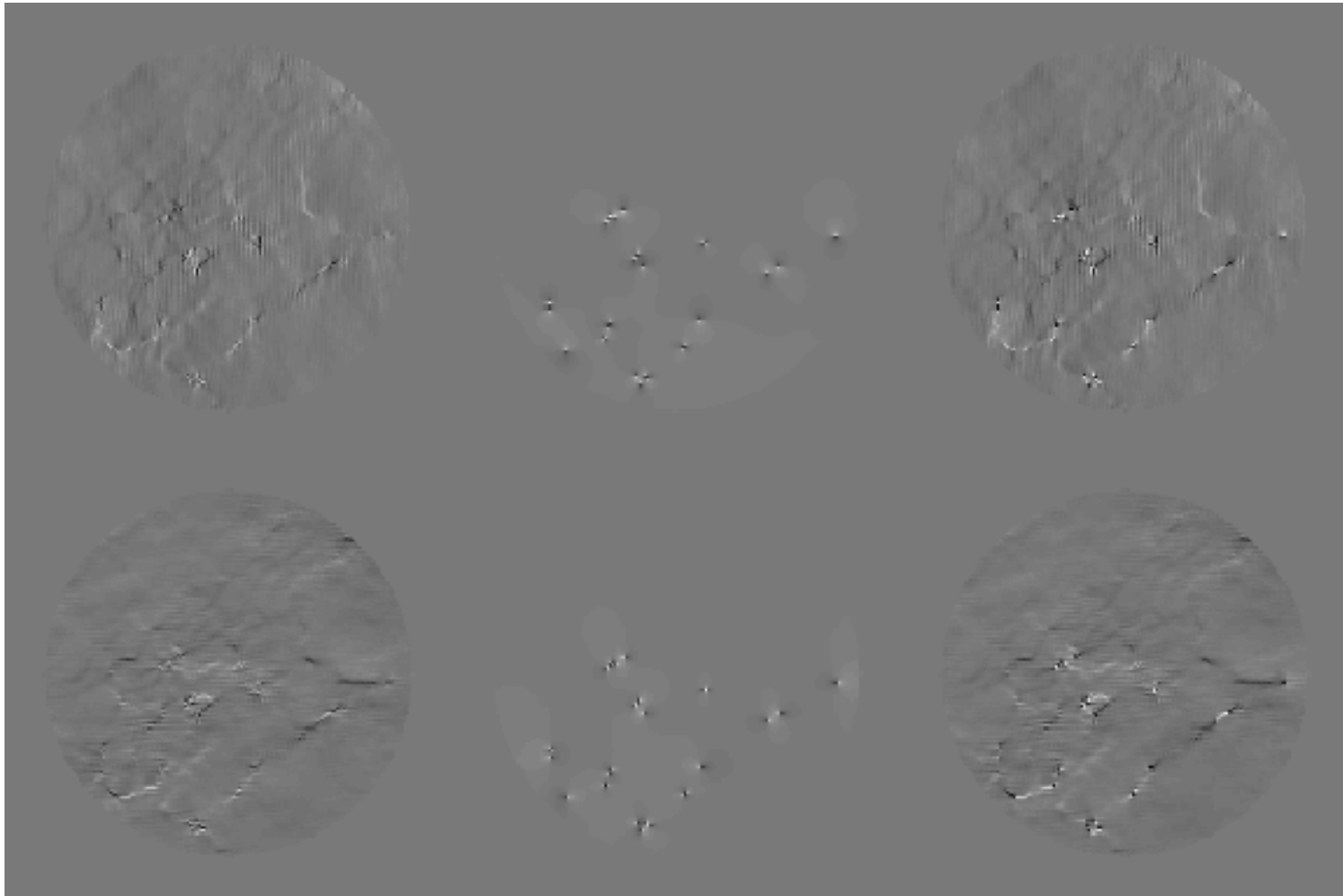
Least Squares

Slope Discrepancy

Total

X-gradients

Y-gradients

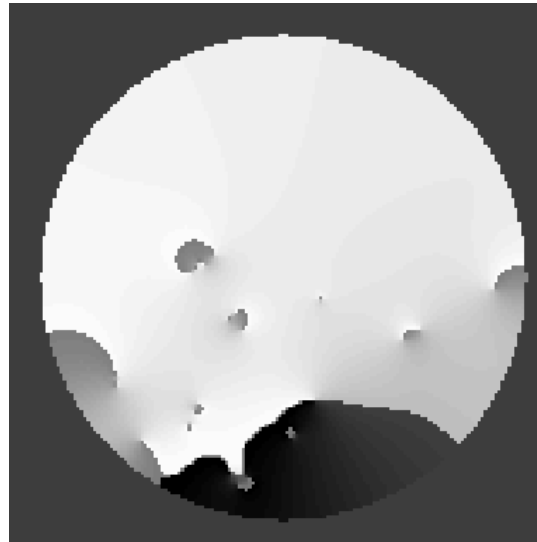


Components of Reconstructed Phase

Least Squares
Strehl = 0.3279



Slope Discrepancy
Strehl = 0.0022



Total
Strehl = 0.9230



- Branch Point locations are automatically reflected in reconstructed Slope Discrepancy phase
- Slope Discrepancy Phase results in very little compensation on it's own, yet when combined with Least Squares component dramatic improvement is achieved
- Branch Point Strehl = 0.3651
- Estimated Least Squares Strehl is $0.9230 * 0.3651 = 0.3359$ which compares favorably with actual Least Square Strehl of 0.3279
- Uncompensated Strehl = 0.0003

X-Gradient Fields with Slope Discrepancy Correction

Iteration 1

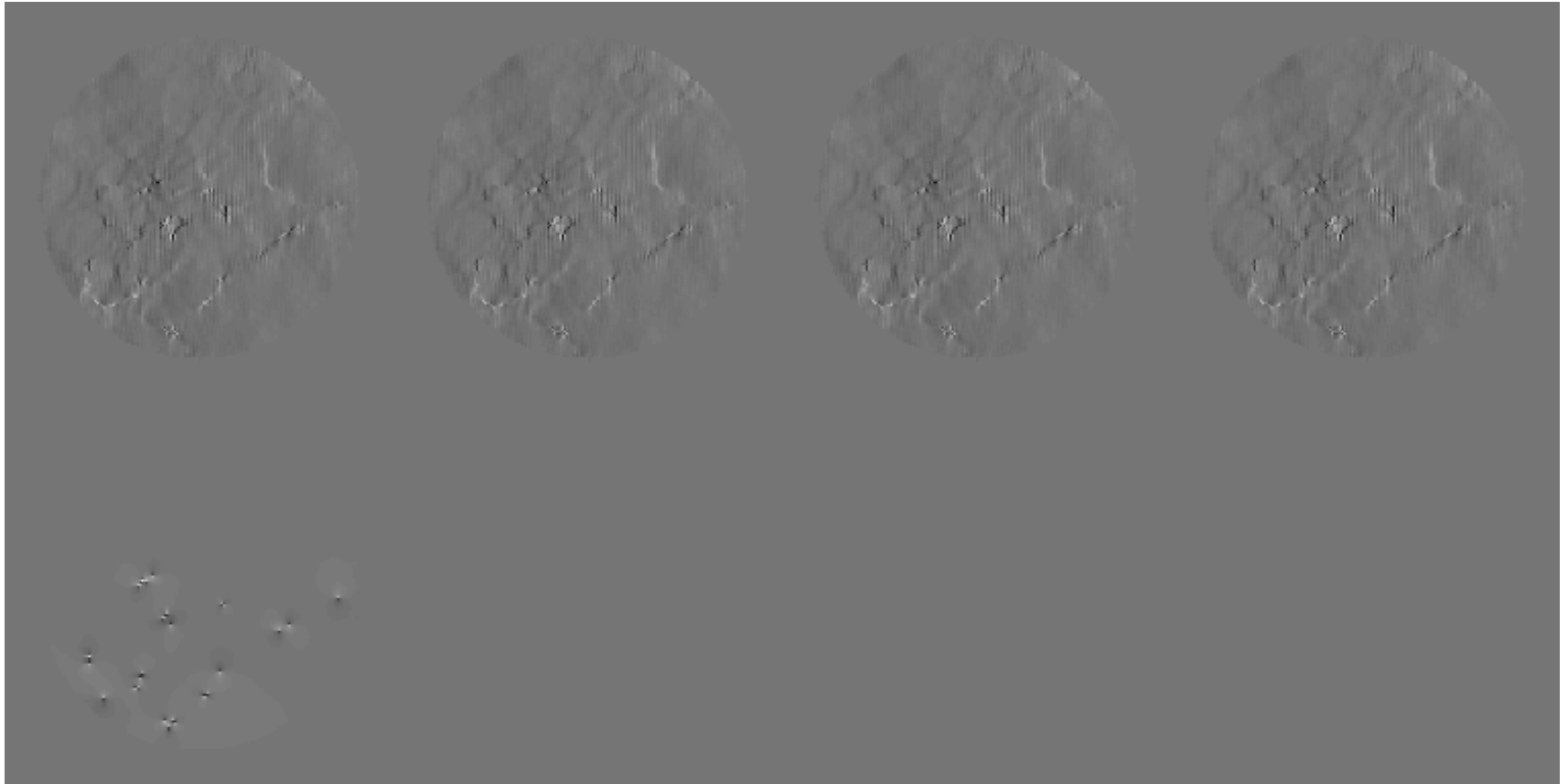
Iteration 2

Iteration 4

Iteration 8

Least
Squares

Slope
Discrepancy



- Turbulence Strength 2 x Clear 1
- Slopes are viewed only through Slope Discrepancy correction

X-Gradient Fields in Closed Loop Operation (Only Least Square Component Applied)

Iteration 1

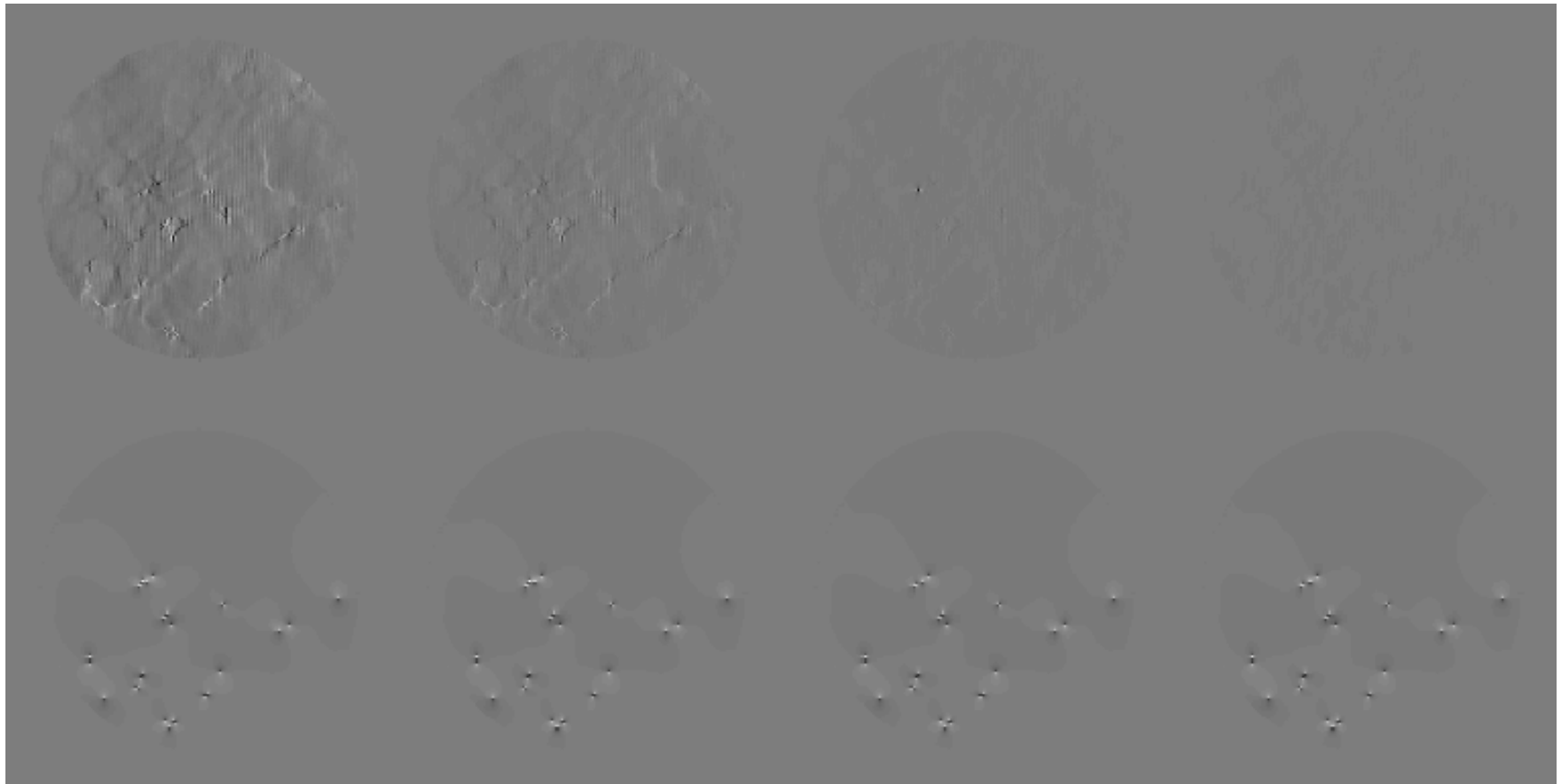
Iteration 2

Iteration 4

Iteration 8

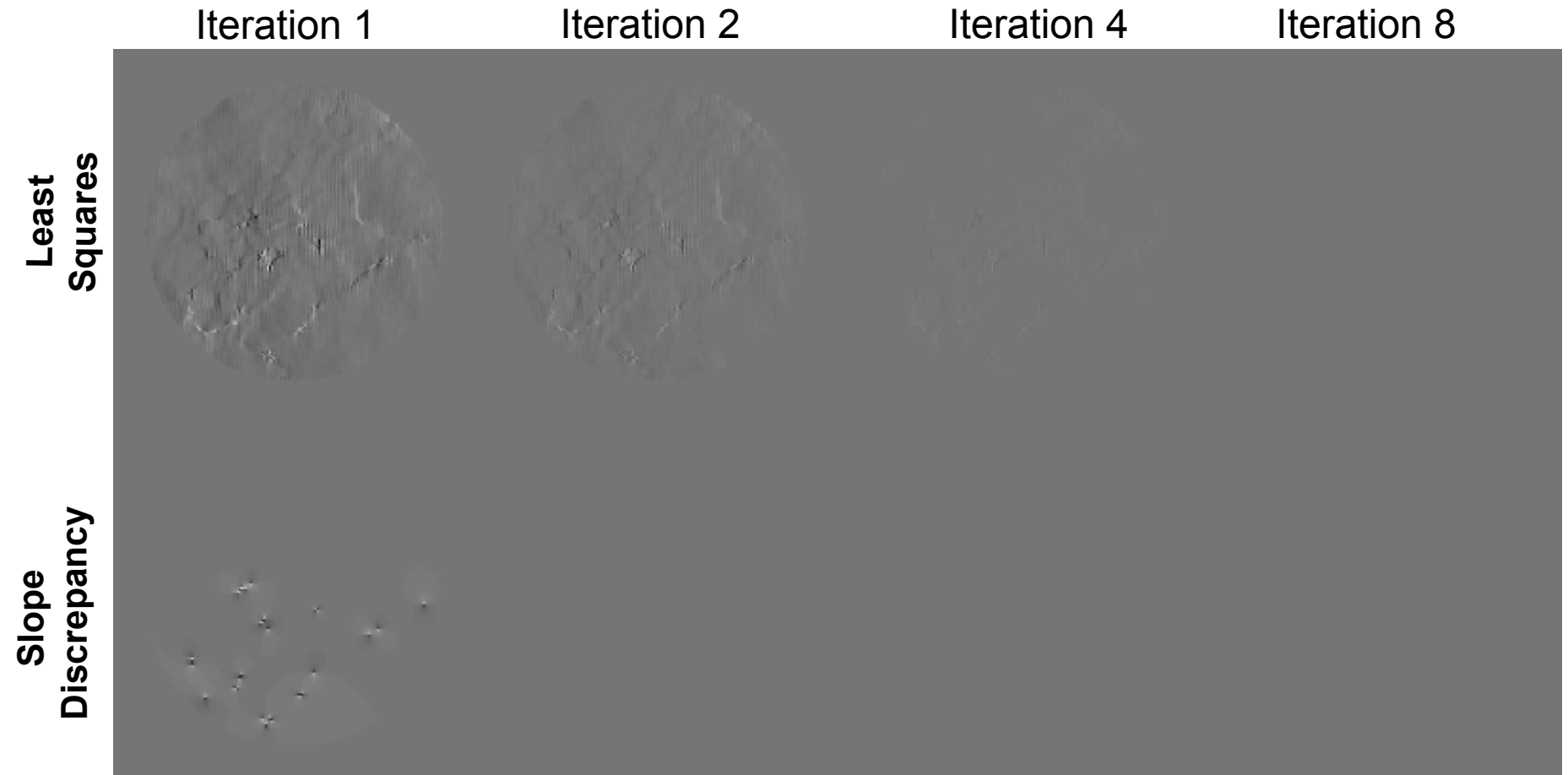
Least
Squares

Slope
Discrepancy



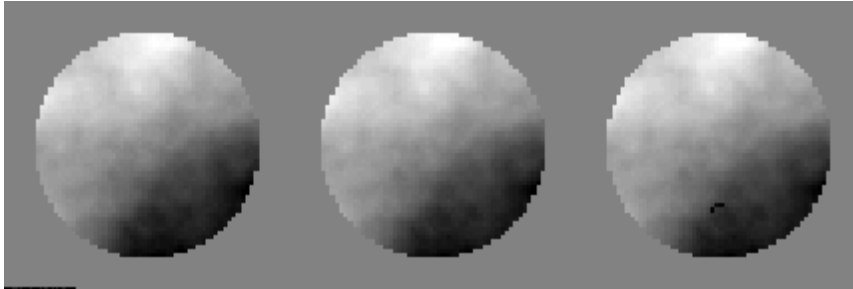
- Control Law Parameters: $a = 1.0$, $b = 0.5$
- Turbulence Strength 2 x Clear 1
- Slopes are viewed only through Least Squares correction

X-Gradient Fields in Closed Loop Operation (Both Components Applied)

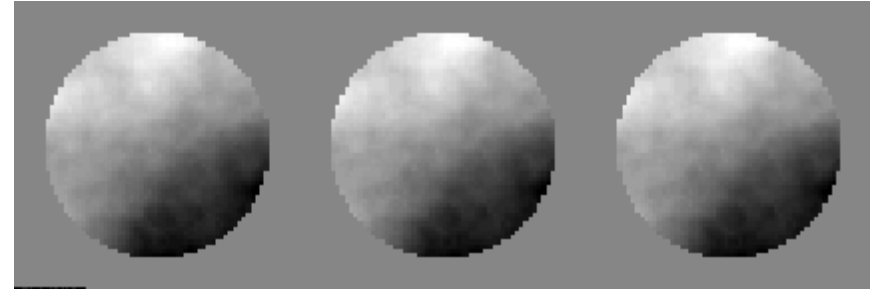


- Control Law Parameters: $a = 1.0$, $b = 0.5$ (LS); $a = 1.0$, $b = 1.0$ (SD)
- Turbulence Strength 2 x Clear 1
- Slopes are viewed through both corrections

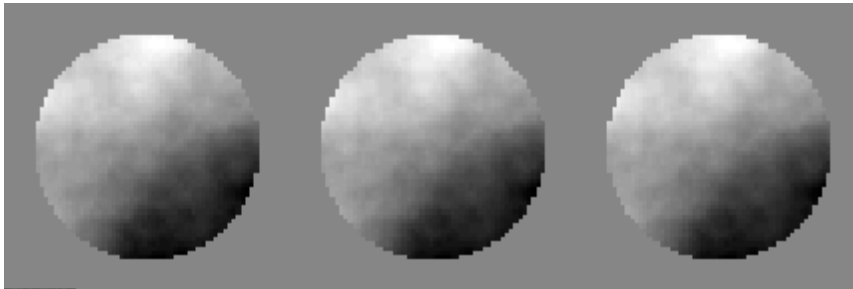
Sample Reconstructed Phase (1992 Phase Points)



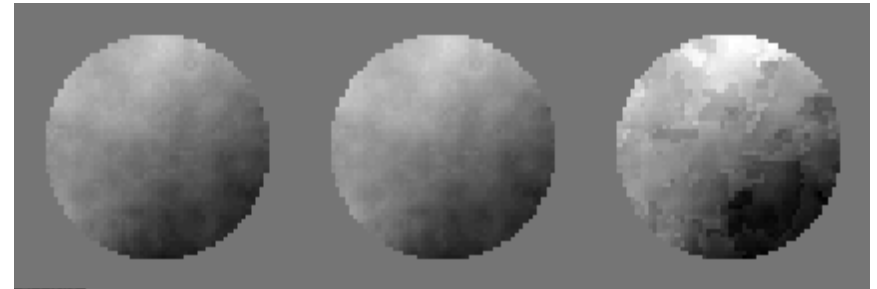
0°



45°



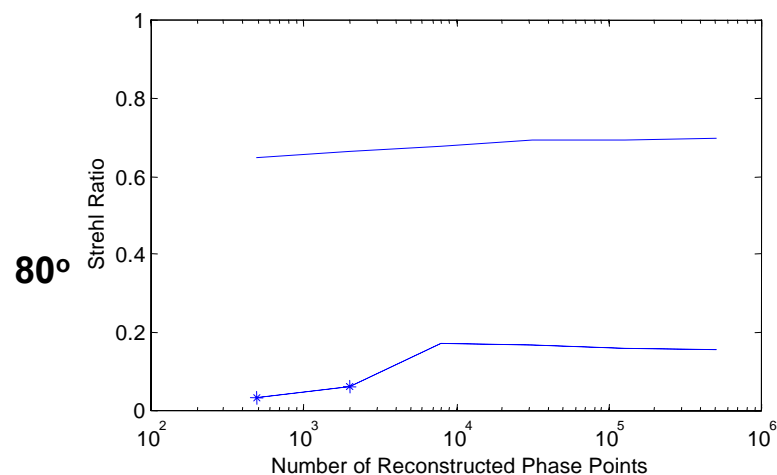
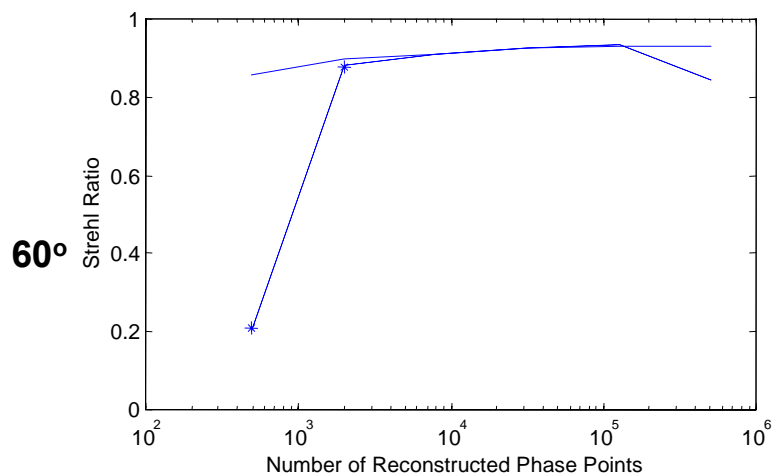
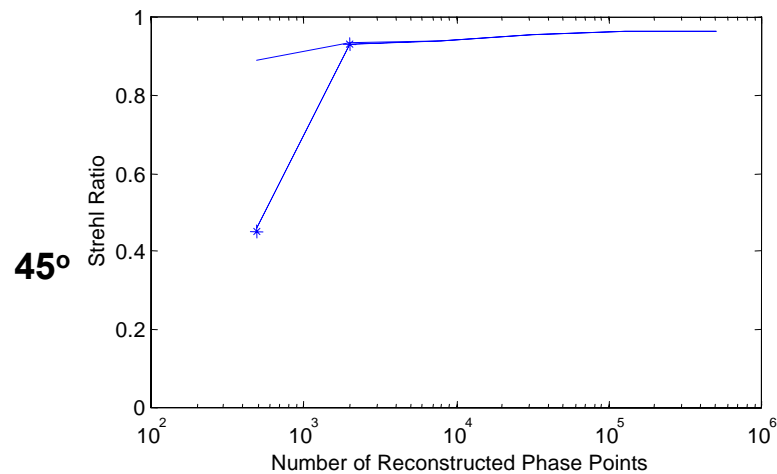
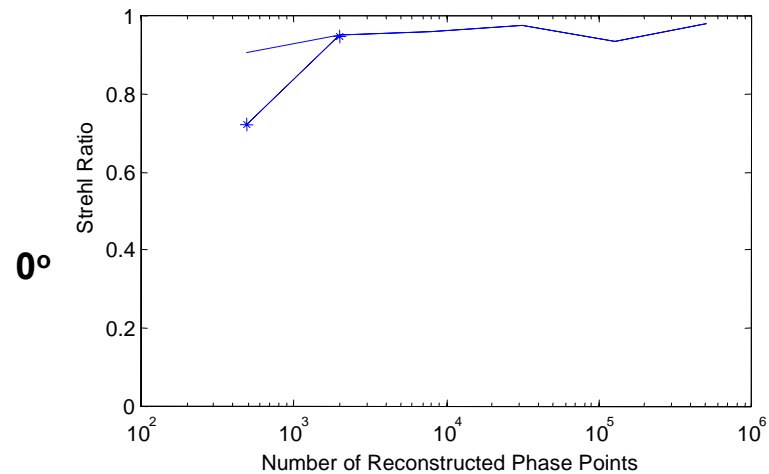
60°



80°

From Left to Right - Matrix Multiply, Fast Least Squares, Branch Cut

Reconstructor Performance (HV_{5/7}, Mean of 10 Realizations)



Solid Line - Branch Cut

Dotted Line - Fast Least Squares

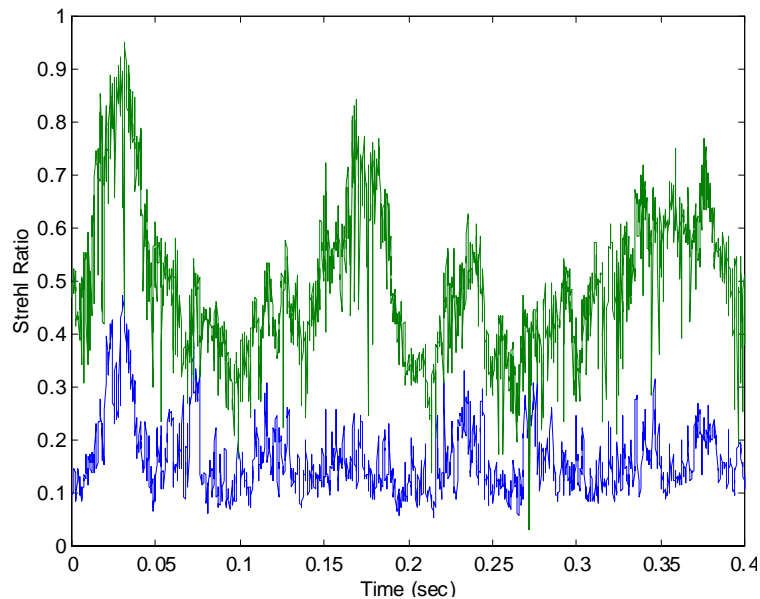
Star - Matrix Multiply

Note: The 500,000x500,000 Fast Least Squares and Branch Cut Reconstructors were implemented by R-Phase

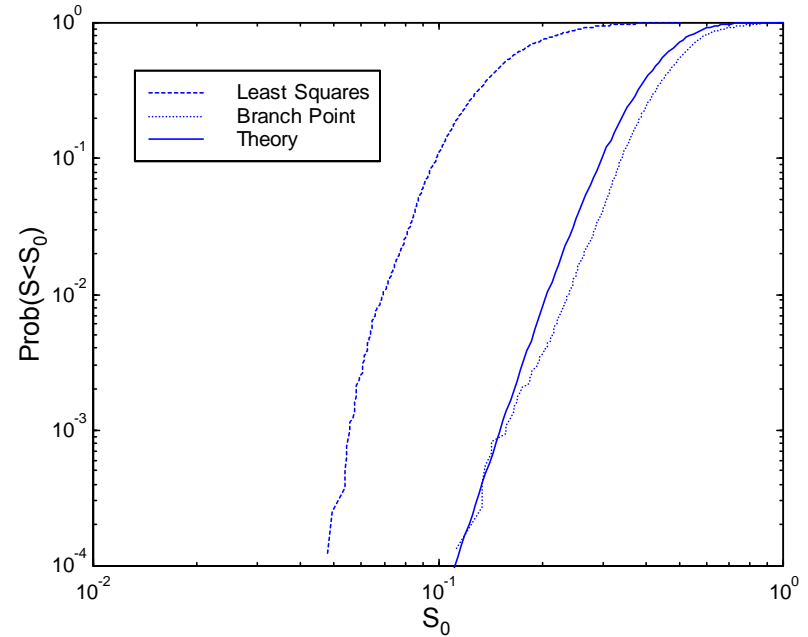
BC-1450

- 17 -

Branch Cut Reconstructor Improves Strehl Variability

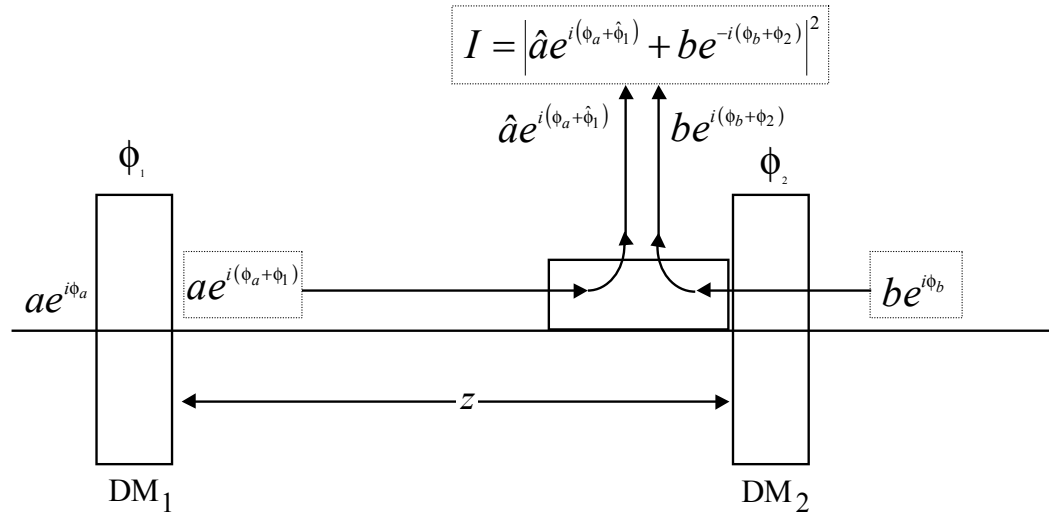


Top Curve : Branch Point Reconstructor
Bottom Curve : Least Squares Reconstructor



- Strehl variability is important in the evaluation of system robustness for an adaptive optics laser transmitter weapon or communication system
- The Branch Cut reconstructor dramatically reduces variability

Multi Conjugate AO Laser Transmitter System: tOSC Baseline MCAO Field Conjugator Concept



- The phase on DM1 (ϕ_1) is adjusted to redistribute the transmitted Irradiance to that of the beacon
- The phase on DM2 (ϕ_2) is adjusted to clean up the diffraction induced wavefront distortion and provide compensation for propagation through the atmosphere
- A third DM may be required to implement the branch point contribution to the phase
- A key feature of this compensation system is the fact that the single wavefront sensor should be made to measure the sum of the phases, $\phi_a + \phi_1 + \phi_b + \phi_2$ (which means that the conjugate of one of the interfering beams must be formed before the beams are combined)
- The correction that nulls this quantity results in the following update

$$\phi_2 = -\phi_a - \hat{\phi}_1 - \phi_b, \quad V = \hat{a}e^{i(\phi_a + \hat{\phi}_1)}e^{i\phi_2} = \hat{a}e^{i(\phi_a + \hat{\phi}_1)}e^{-i(\phi_a + \hat{\phi}_1 + \phi_b)} = \hat{a}e^{-i\phi_b} = be^{-i\phi_b}, \quad \hat{a} = b$$

- The measurement $\log(a) - \log(b)$ is nulled to determine the phase on DM1

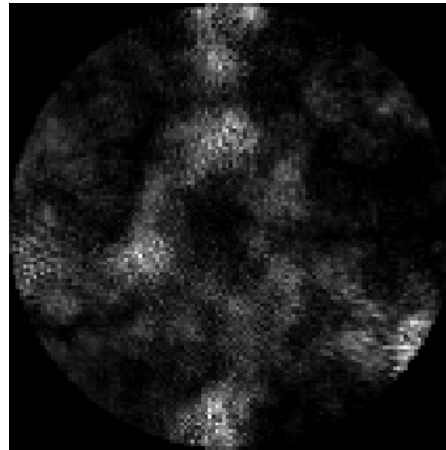
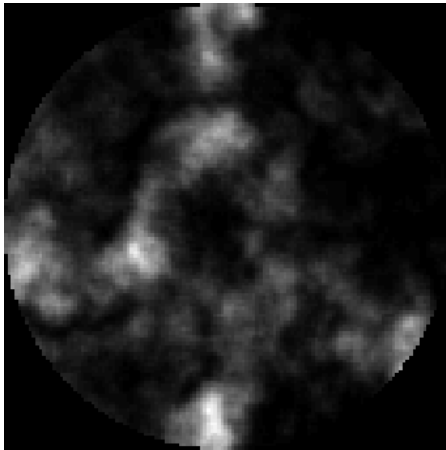
2 DM Field Conjugation Point Source Results: Irradiance Profiles and Performance

Beacon Pupil Plane Intensity

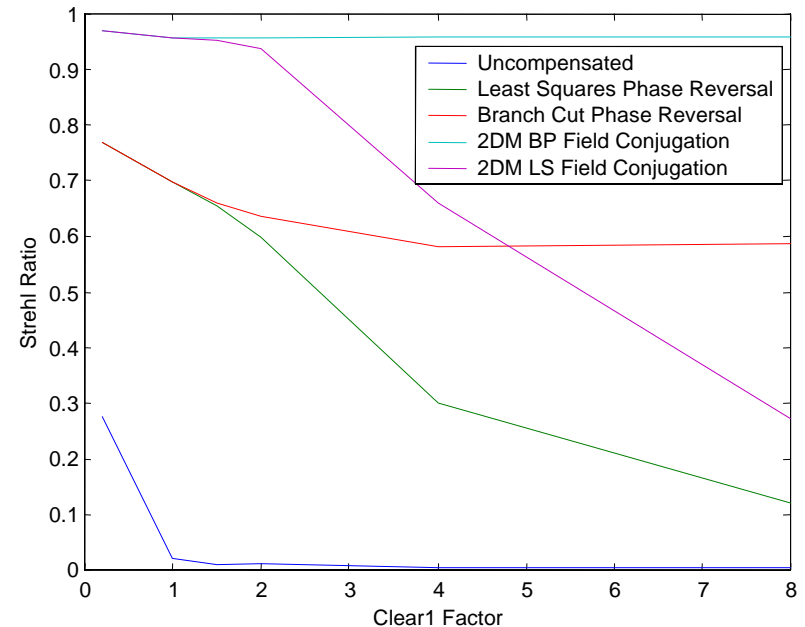
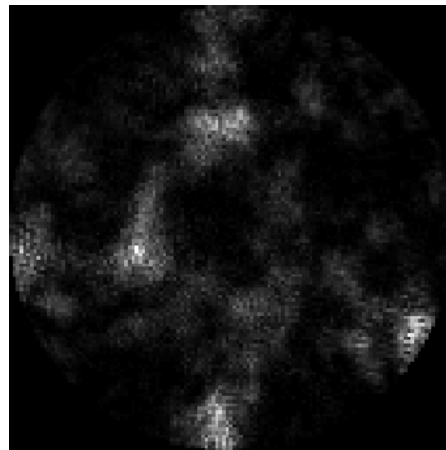
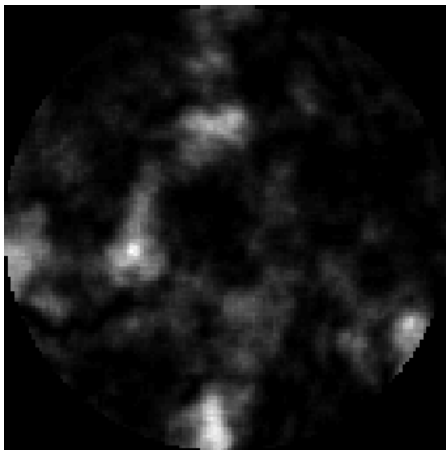
Reconstructed Intensity at the Pupil Plane

Strehl Ratio Performance Using 20 Iteration GS Solver

2 x Clear1



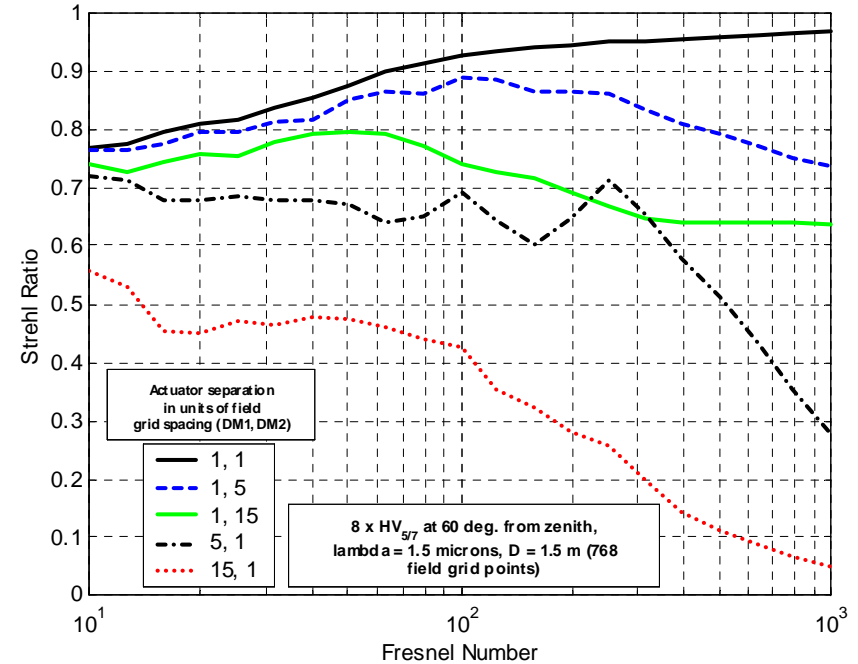
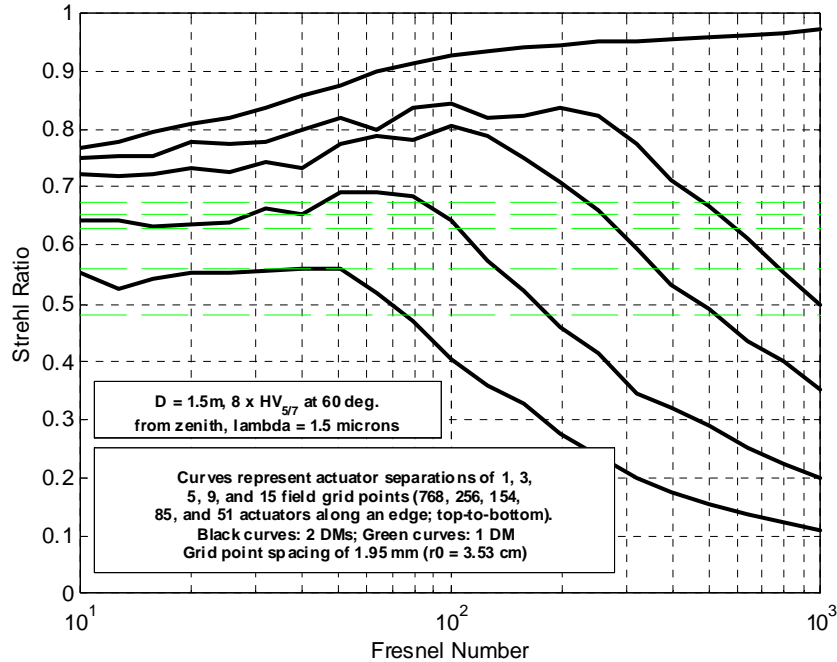
4 x Clear1



NOP Like Configuration:

- Aperture Diameter, $D=0.75\text{m}$
- Propagation wavelength, $\lambda = 1.06\mu\text{m}$
- C_n^2 Constant over 50km range
- Single Correction with unity gain
- Full Field Resolution Correction (128 point across aperture)

Impact of Fitting Errors for Uplink Propagation for GS MCAO



- In high turbulence, MCAO is superior to single DM if:
 - Adequate number of actuators
 - Judicious choice of N_f
- High actuator densities more important on DM_2 than DM_1 (phase reversal more important than matching beacon amplitude)

Maximum Power Transfer Beam Fields Satisfy an Energy Eigenvalue Equation

- Utilize Operators in Abstract Hilbert space to represent relationship between transmitted and received fields

- For propagation to the receiver plane

$$|v\rangle = F|a\rangle, F = W_2 G W_1, W_2|v\rangle = |v\rangle, W_1|a\rangle = |a\rangle, G^\dagger G = I,$$

$$\langle r|G|a\rangle = \langle r|G\left(\int du|u\rangle\langle u|\right)|a\rangle = \int du\langle r|G|u\rangle\langle u|a\rangle = \int duG(u,r)a(u),$$

$$\langle a|a\rangle = \langle a|\left(\int du|u\rangle\langle u|\right)|a\rangle = \int du\langle a|u\rangle\langle u|a\rangle = \int du a^*(u)a(u)$$

- The efficiency can be expressed as the following operator expression

$$\varepsilon = P/P_0 = \frac{\langle v|v\rangle}{\langle a|a\rangle} = \frac{\langle a|F^\dagger F|a\rangle}{\langle a|a\rangle} = \frac{\langle a|H|a\rangle}{\langle a|a\rangle}, H = F^\dagger F = W_1^\dagger G^\dagger W_2^\dagger W_2 G W_1 = W_1^\dagger G^\dagger W_2 G W_1, W_n^\dagger W_n = W_n = W_n^\dagger$$

- LaGrange Multipliers are used to determine the maximum power transfer beam fields

$$P = \langle a|H|a\rangle + \varepsilon(P_0 - \langle a|a\rangle),$$

$$\frac{\partial P}{\partial \varepsilon} = P_0 - \langle a|a\rangle = 0 \Rightarrow P_0 = \langle a|a\rangle, \frac{\partial P}{\partial \langle a|a\rangle} = H|a\rangle - \varepsilon|a\rangle = 0 \Rightarrow H|a\rangle = \varepsilon|a\rangle$$

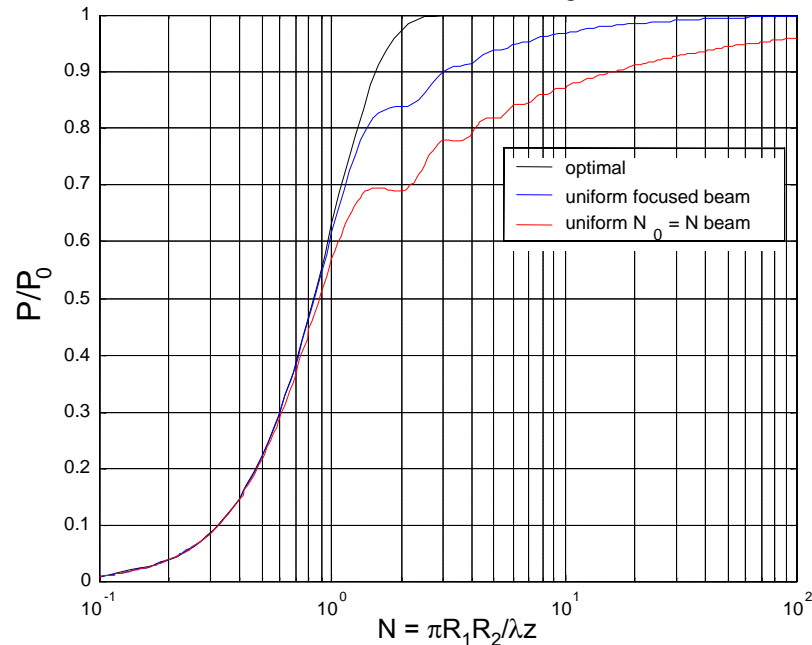
$$\therefore \langle a|H|a\rangle = \varepsilon\langle a|a\rangle, \varepsilon = \frac{\langle a|H|a\rangle}{\langle a|a\rangle} = \frac{P}{P_0}, P = \langle a|H|a\rangle$$

- The efficiency is optimized by launching the field that corresponds to the eigenvector of the operator H with the largest “energy” eigenvalue
- For Free space propagation in discrete Fresnel approximation

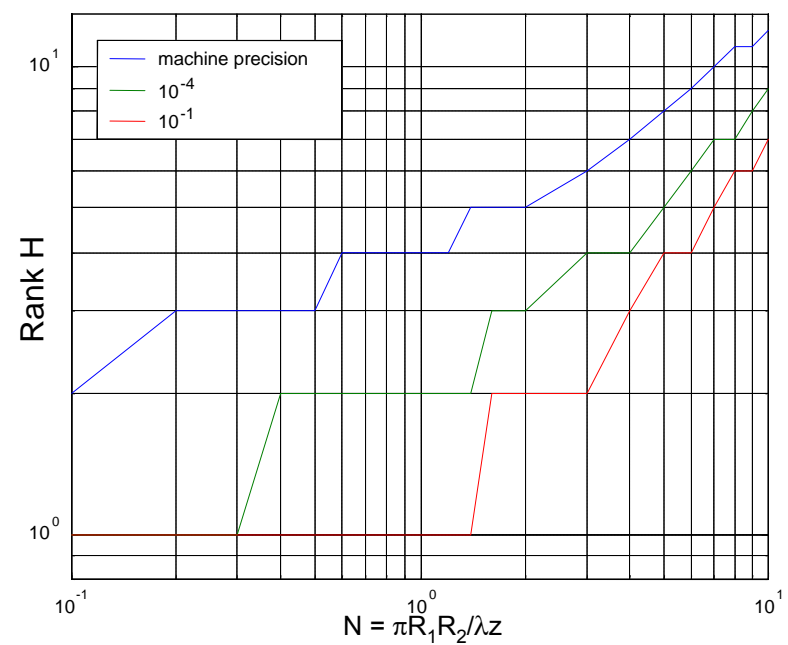
$$\langle \alpha_n | e \rangle = \sqrt{\frac{2\alpha_n \pi R_1^2}{\tilde{N}}} A(\alpha_n R_1) \exp(iN_0 \alpha_n^2), \langle \alpha_n | H | \alpha_m \rangle = \frac{4N^2 \sqrt{\alpha_n \alpha_m}}{\tilde{N}^2} \sum_{l=1}^{\tilde{N}} \rho_l J_\nu(2N\rho_l \alpha_n) J_\nu(2N\rho_l \alpha_m), n, m = 1, 2, \dots, \tilde{N}$$

Efficiency and Information Content of Beam Field Increases Monotonically with Fresnel Number and Rank of Power Operator

Efficiency

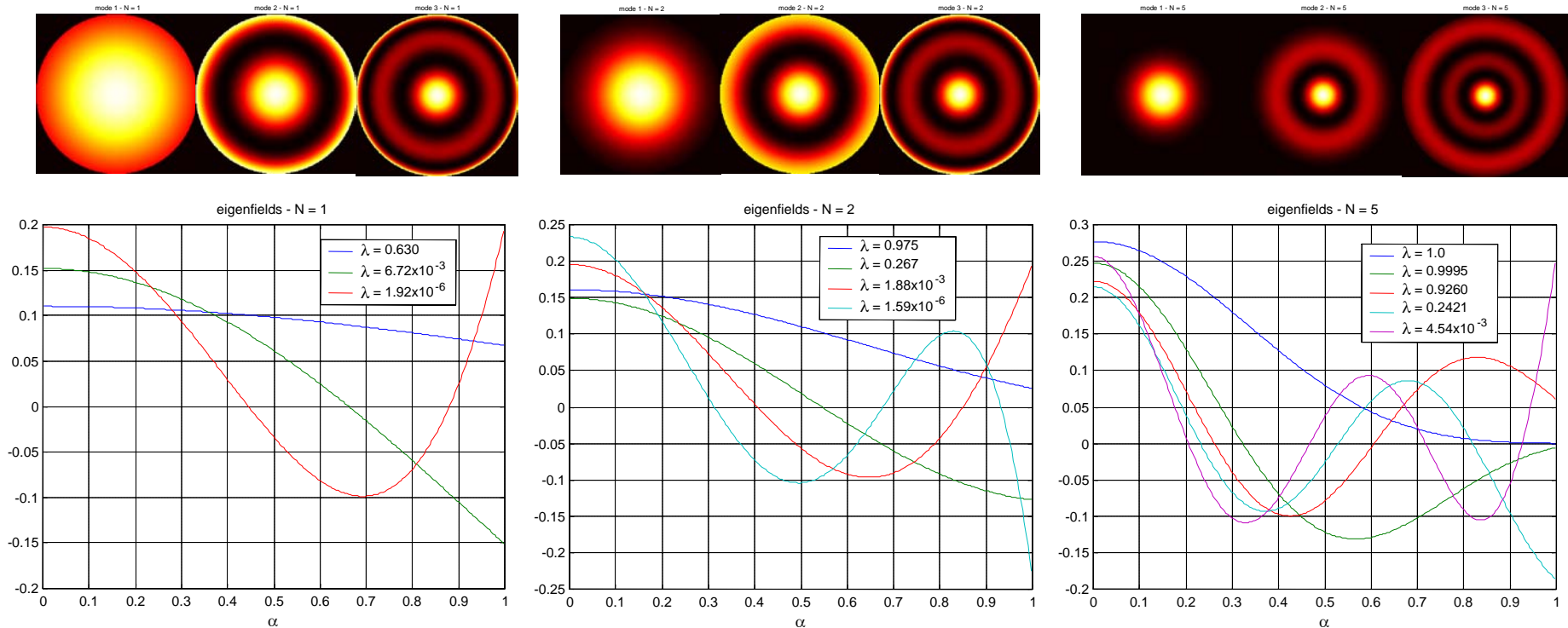


Operator Rank



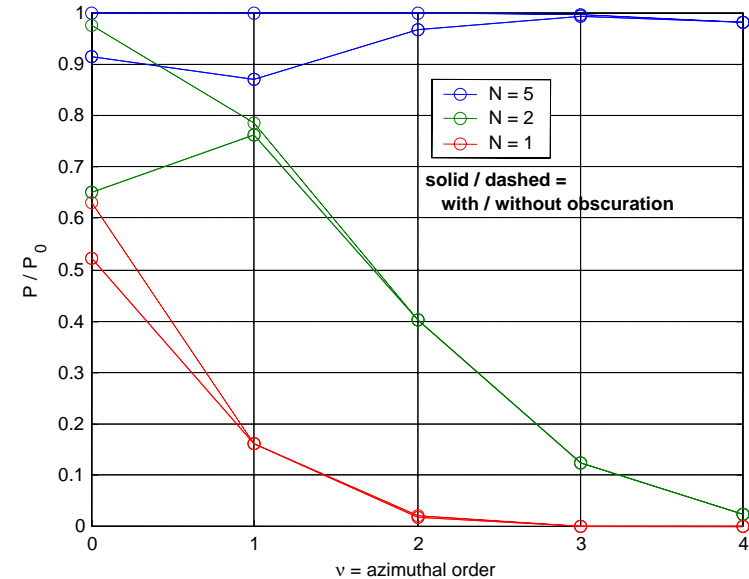
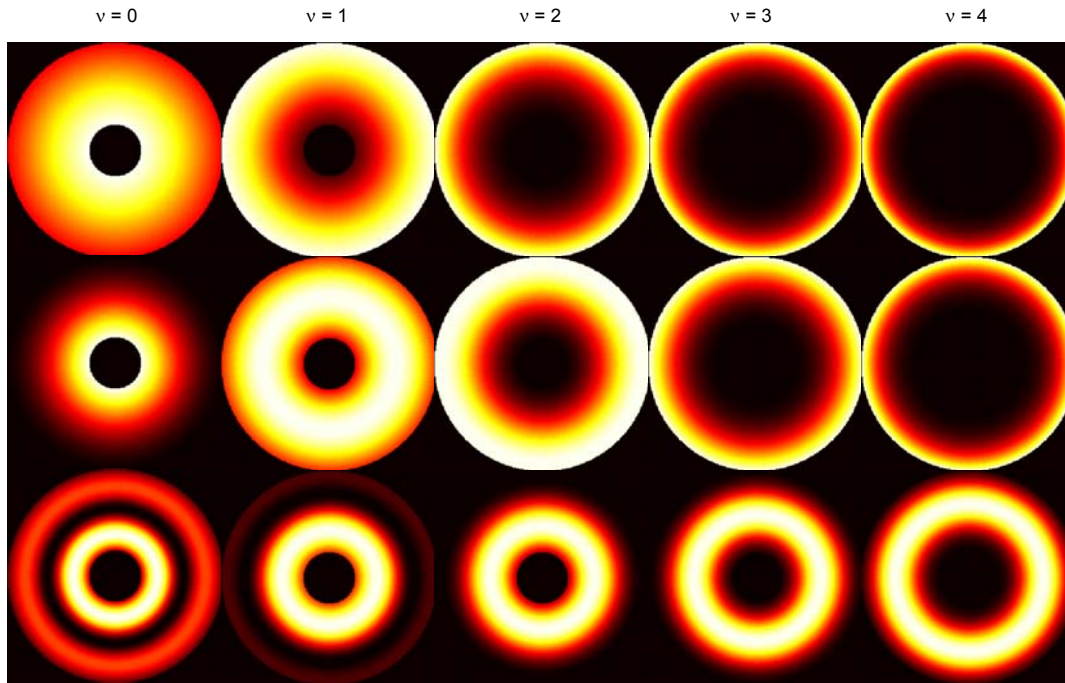
- Information content (and rank of the operator) of beam field increases monotonically with Fresnel number
- $N_0=0$ Beam Fields provide viable options for all Fresnel numbers
- Geometrical optics containment ($N=N_0$) may not require Irradiance redistribution (or AO) but it provides low efficiency in the critical range $1 < N < 10$

Free Space Maximum Efficiency Eigenfields are Nearly Gaussian Beams for Fresnel Numbers of Interest



- Top figures illustrate the first three eigenfields corresponding to propagation Fresnel numbers $N=1,2,5$
- Graphs illustrate radial plots and eigenvalues for the eigenvectors
- For $N=1,2,5$ only one, two and four modes are supported by the relay link
- As the propagation Fresnel number increases, less of the aperture is used to provide natural guardband to ensure efficiency

Maximum Efficiency Vector Bessel Beams Can Accommodate a Central Obscuration



- Vector Bessel Beams have the functional form $f_v(r)\exp(iv\theta)$
- The highest order radial mode for each of the first five azimuthal orders is illustrated above for a variety of propagation Fresnel numbers
- Central Obscuration ratio of 4.3 can be accommodated by higher order Vector Bessel beam if propagation Fresnel number is high enough to contain required information content

Assessment of Levy-Stark Beam Field Concepts

- Levy-Stark (LS) Beam Fields (proposed by Jeff Barchers, studied by Fried, Butts, Tyler, etc.)
 - These fields represent dual converged closed loop AO compensated states for both beacon and transmitter (Both HEL and Beacon are compensated)
 - For field conjugation correction the closed loop fields correspond to the modes of a resonator with phase conjugate mirrors and are solutions of the following operator equation

$$|u\rangle = F^\dagger |v\rangle = F^\dagger F |a\rangle = H |a\rangle = \lambda |a\rangle \Rightarrow H |e_n\rangle = \lambda_n |e_n\rangle$$

- This is the same eigenvalue expression as that required to minimize the energy loss
- Levy-Stark Theorem confirms control system convergence to a local minimum but AO convergence is based on Power method
- For field conjugation correction eigenanalysis illustrates convergence to absolute minimum and provides insight to convergence rate

- Arbitrary starting solution is represented as a superposition of eigenvectors

$$|f\rangle = \sum_n a_n |e_n\rangle, H |e_n\rangle = \epsilon_n |e_n\rangle, P_0 = \langle f | f \rangle = \sum_{n,m} a_m^* a_n \langle e_m | e_n \rangle = \sum_{n,m} a_m^* a_n \delta_{nm} = \sum_n |a_n|^2$$

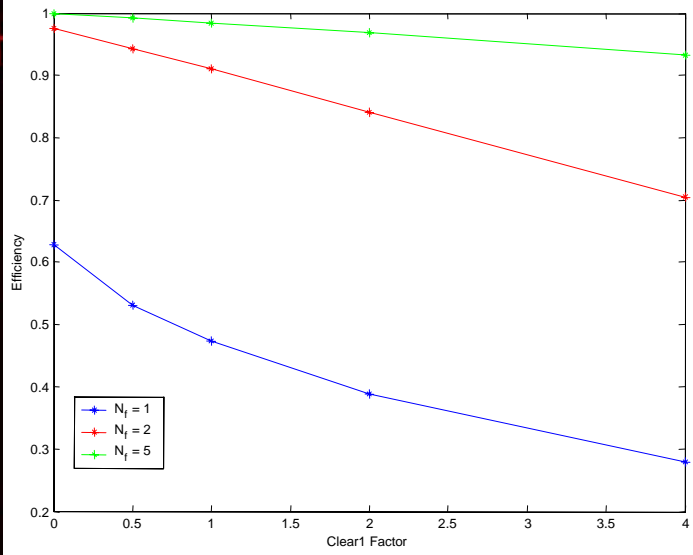
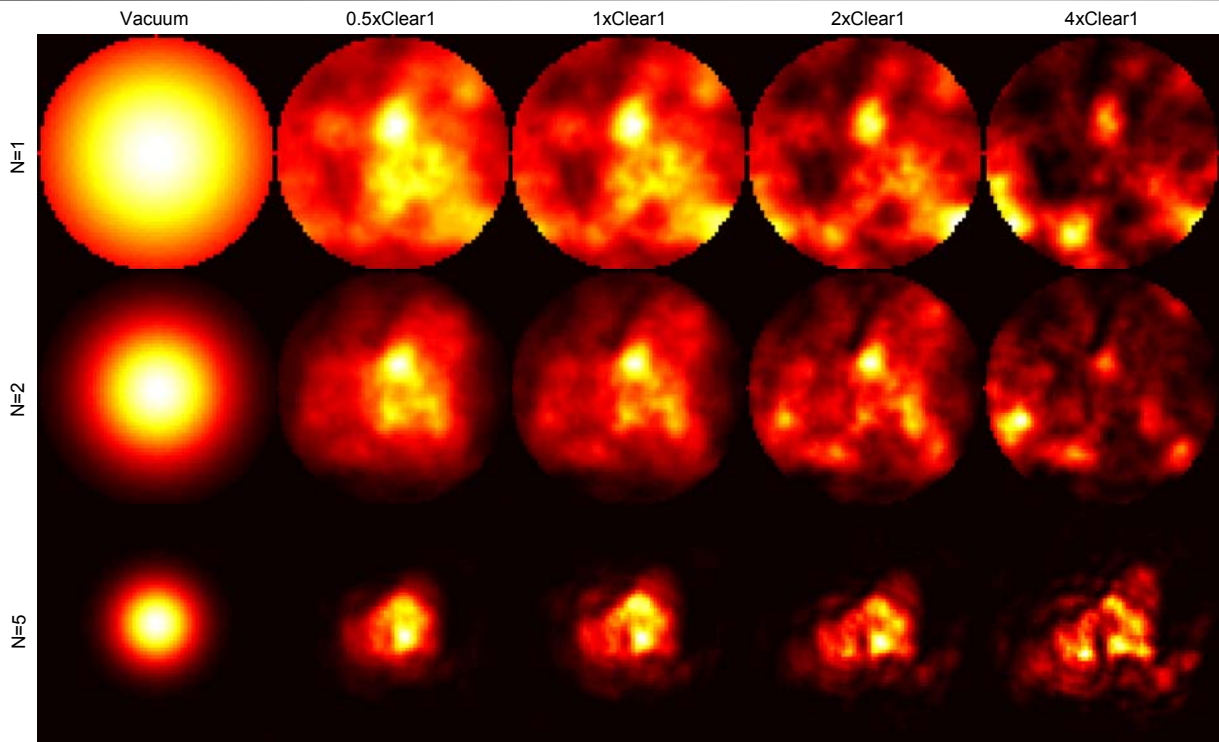
- After N AO correction iterations

$$H^N |f\rangle = \sum_n a_n H^N |e_n\rangle = \sum_n a_n \epsilon_n^N |e_n\rangle = \epsilon_1^N \sum_n a_n \left(\frac{\epsilon_n}{\epsilon_1}\right)^N |e_n\rangle, P_0 = \epsilon_1^{2N} \sum_n \left(\frac{\epsilon_n}{\epsilon_1}\right)^{2N} |a_n|^2$$

- For large enough N all the power is in the mode with the maximum eigenvalue which maximizes the transmitted power
- For modes with closely spaced eigenvalues the convergence rate and its implications can be assessed in detail

Maximum Efficiency Eigenfields in the Presence of a Single Turbulence Realization

($P=1$ Watt, $D_T = 1.5$ m, $D_R = 1.5$ m, $2 \times \text{Clear1}$, Transmitter at $h_T = 12$ km, Receiver at $h_R = 29$ km, Range = 267 km, $\lambda = 1.3 \mu\text{m}$, Grid Branch Cut AO at Transmitter and Relay)



- Nominal propagation Fresnel number is $N=5$
- Fresnel number changed by reducing mirror diameters keeping propagation and turbulence consistent
- Eigenfield solutions for higher Fresnel numbers attempt to maintain natural guard band to minimize energy loss

Optimum Efficiency Beam Field Perturbation Approach

- In the presence of a given turbulence realization the minimum energy loss beam fields follow a similar eigenvalue equation

$$H|e_n\rangle = \varepsilon_n|e_n\rangle, H = H^{(0)} + H^{(1)}, H^{(0)} \Rightarrow \text{free space}$$

- To assess the expected efficiency the ensemble average must be evaluated

$$\langle \varepsilon_n \rangle = \langle \langle e_n | H | e_n \rangle \rangle \neq \langle e_n | \langle H \rangle | e_n \rangle$$

- This process is linerized by utilizing perturbation theory

$$\varepsilon_n = \varepsilon_n^{(0)} + \varepsilon_n^{(1)} + \varepsilon_n^{(2)} + \dots, |e_n\rangle = |e_n^{(0)}\rangle + |e_n^{(1)}\rangle + |e_n^{(2)}\rangle + \dots, |e_n^{(l)}\rangle = \sum_{m \neq n} a_{nm}^{(l)} |e_m^{(0)}\rangle, a_{nm}^{(l)} = \langle e_m^{(0)} | e_n^{(l)} \rangle$$

$$H^{(0)}|e_n^{(0)}\rangle = \varepsilon_n^{(0)}|e_n^{(0)}\rangle \quad \text{unperturbed vacuum states}$$

$$H^{(0)}|e_n^{(1)}\rangle + H^{(1)}|e_n^{(0)}\rangle = \varepsilon_n^{(0)}|e_n^{(1)}\rangle + \varepsilon_n^{(1)}|e_n^{(0)}\rangle \quad \text{first order}$$

$$H^{(0)}|e_n^{(2)}\rangle + H^{(1)}|e_n^{(1)}\rangle = \varepsilon_n^{(0)}|e_n^{(2)}\rangle + \varepsilon_n^{(1)}|e_n^{(1)}\rangle \quad \text{second order}$$

- Forming the appropriate inner products results in the following solution

$$\varepsilon_n^{(1)} = \langle e_n^{(0)} | H^{(1)} | e_n^{(0)} \rangle, \langle e_m^{(0)} | e_n^{(1)} \rangle = \frac{\langle e_m^{(0)} | H^{(1)} | e_n^{(0)} \rangle}{\varepsilon_n^{(0)} - \varepsilon_m^{(0)}}, \varepsilon_n^{(2)} = - \sum_{l \neq n} \frac{\langle e_n^{(0)} | H^{(1)} | e_l^{(0)} \rangle \langle e_l^{(0)} | H^{(1)} | e_n^{(0)} \rangle}{\varepsilon_n^{(0)} - \varepsilon_l^{(0)}}, \langle e_m^{(0)} | e_n^{(1)} \rangle = - \frac{\langle e_n^{(0)} | H^{(1)} | e_n^{(0)} \rangle \langle e_m^{(0)} | H^{(1)} | e_n^{(0)} \rangle}{(\varepsilon_n^{(0)} - \varepsilon_m^{(0)})^2} - \sum_{l \neq n} \frac{\langle e_n^{(0)} | H^{(1)} | e_l^{(0)} \rangle \langle e_l^{(0)} | H^{(1)} | e_n^{(0)} \rangle}{(\varepsilon_n^{(0)} - \varepsilon_m^{(0)}) (\varepsilon_n^{(0)} - \varepsilon_l^{(0)})}$$

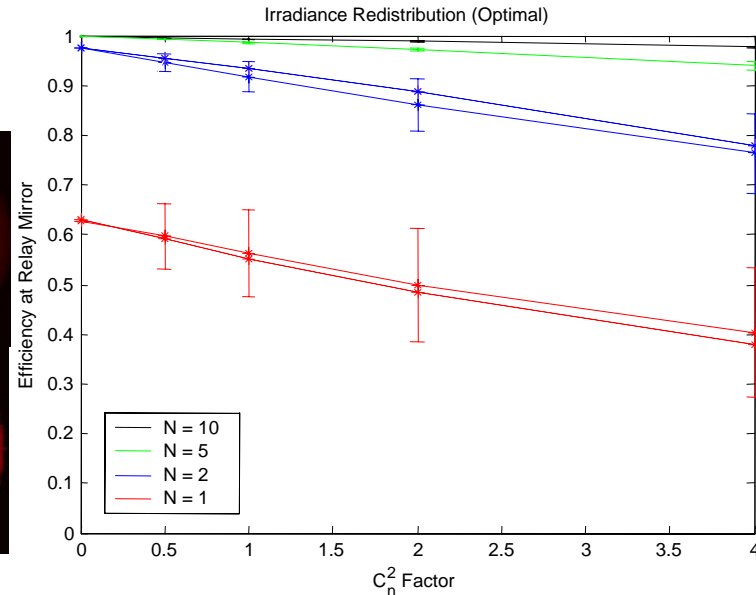
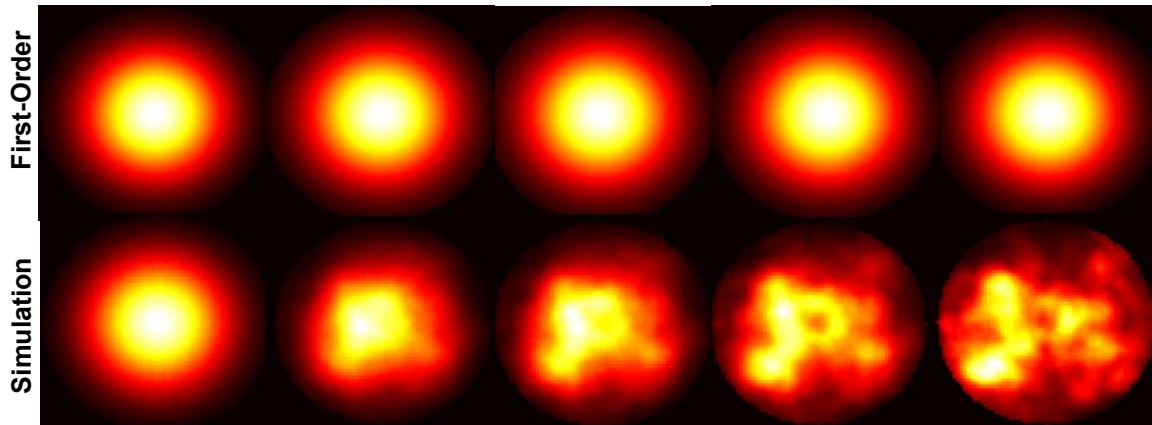
- Up to second order the expected efficiency is

$$\langle \varepsilon_n \rangle = \varepsilon_n^{(0)} + \langle \varepsilon_n^{(1)} \rangle + \langle \varepsilon_n^{(2)} \rangle = \varepsilon_n^{(0)} + \langle e_n^{(0)} | \langle H^{(1)} \rangle | e_n^{(0)} \rangle - \sum_{l \neq n} \frac{\langle \langle e_n^{(0)} | H^{(1)} | e_l^{(0)} \rangle \langle e_l^{(0)} | H^{(1)} | e_n^{(0)} \rangle \rangle}{\varepsilon_n^{(0)} - \varepsilon_l^{(0)}}$$

Comparison of Perturbation Theory and Wave-Optics Simulation for Maximum Efficiency Beam Fields

Ensemble Average First Order Maximum Efficiency Beam Fields

Vacuum 0.5xClear1 1xClear1 2xClear1 4xClear1



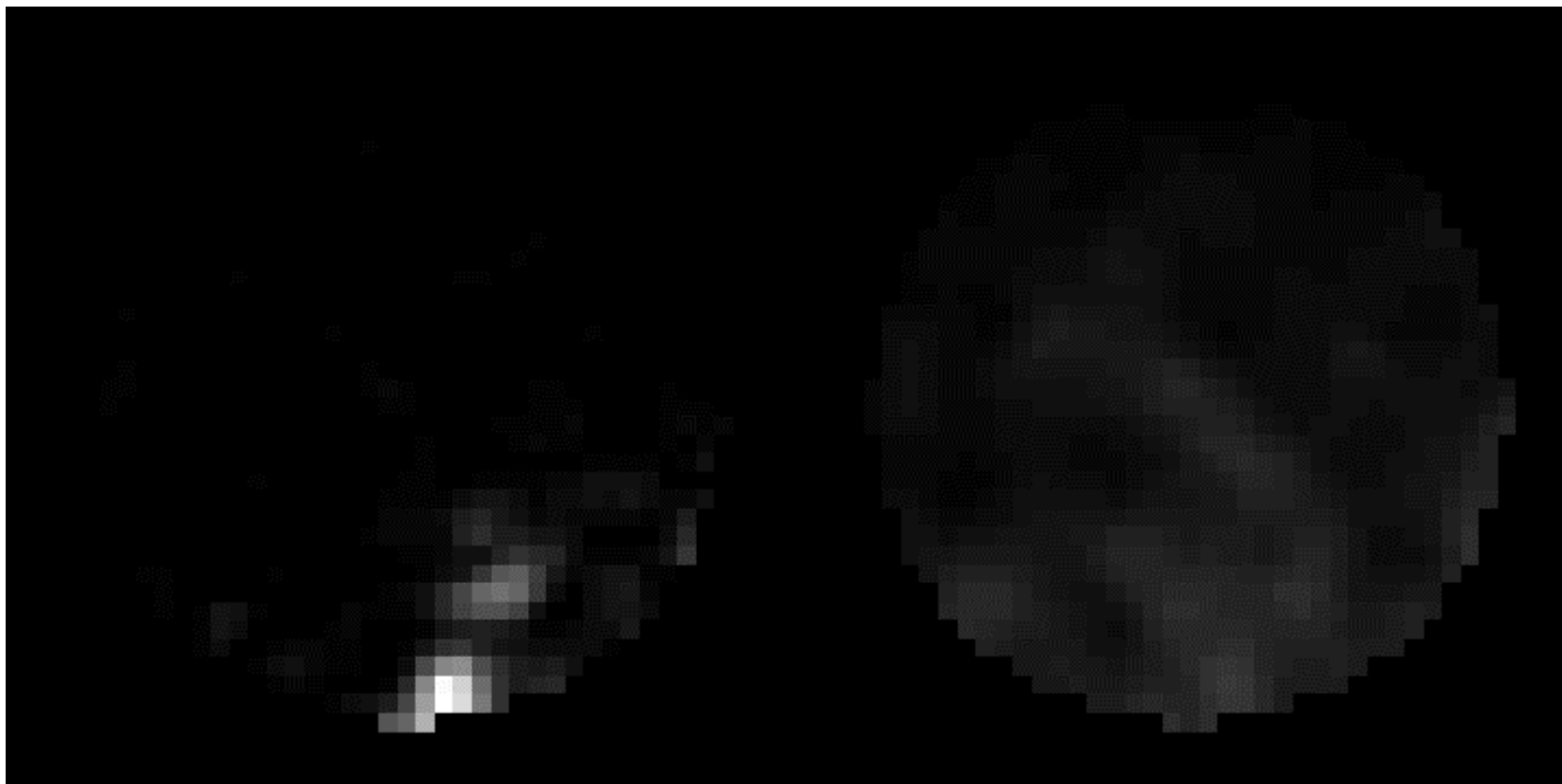
- Initial second order perturbation theory results are in general agreement with average of 16 wave optics simulation realizations (More work is planned to fine tune analysis)
- Dotted curves illustrate second order eigenvalue results
- 16 wave optics realizations provide poor averaging in strong turbulence cases illustrating the benefit of the perturbation analysis approach which illustrates that with good AO compensation of amplitude and phase average field is only weakly perturbed

Plane Wave Parameters for Deep Turbulence

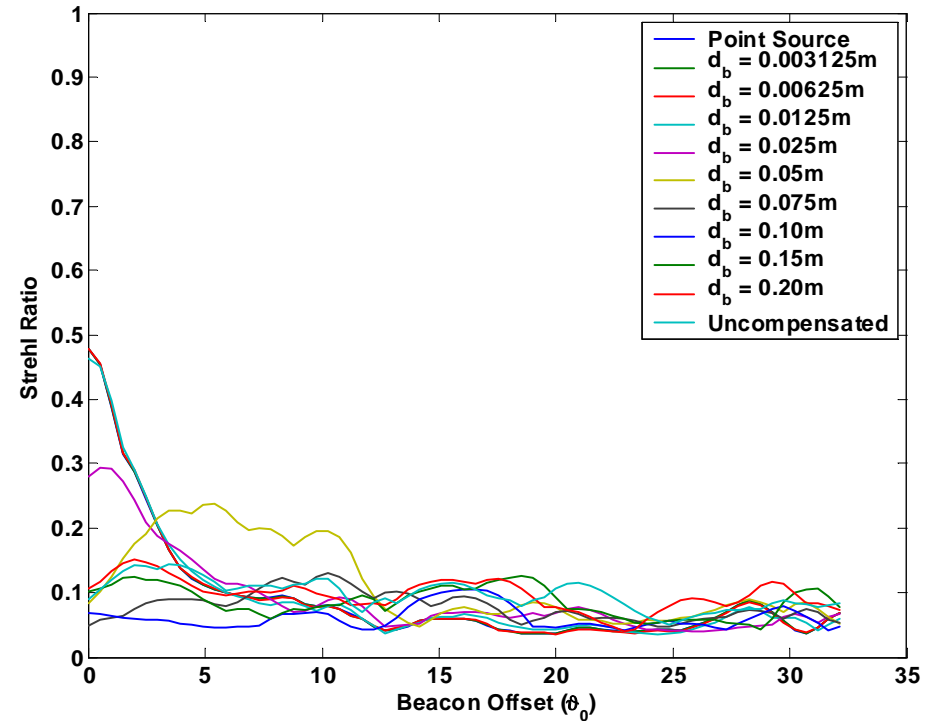
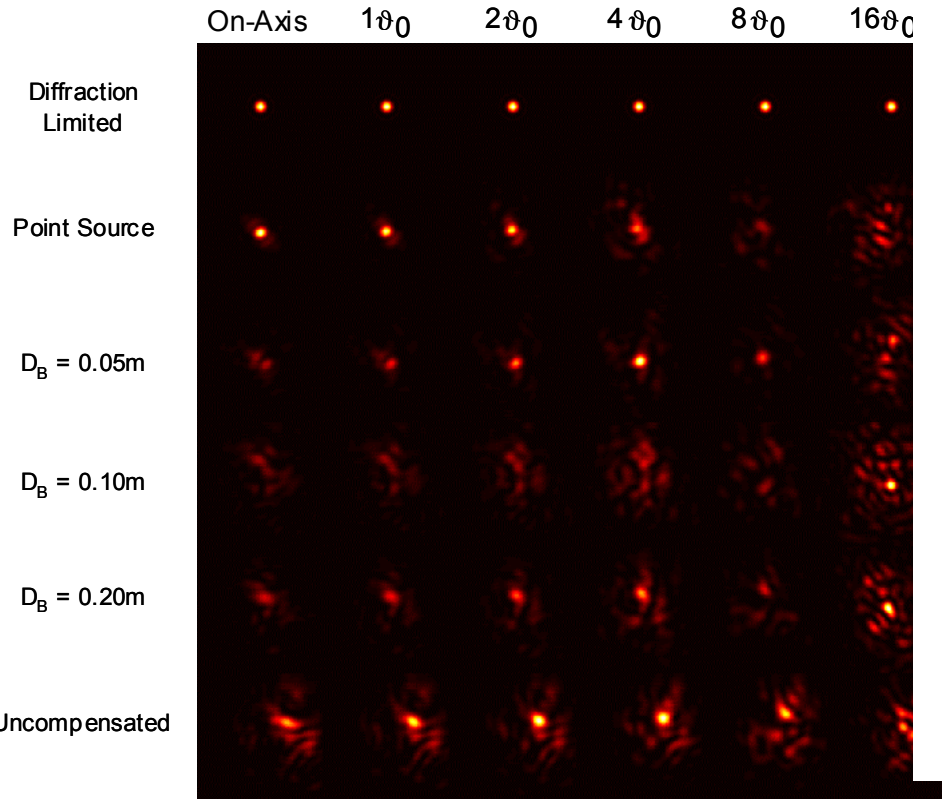
Configuration	Range (km)	C_n^2 ($\text{m}^{-2/3}$)	λ (μm)	D m	r_0 (cm)	ϑ_0 μrad	σ_ℓ^2 (nep)	σ_θ^2 (μrad)
Deep	2	2×10^{-13}	1.06	0.1	0.544	1.54	5.5	49.5
NOP	50	1×10^{-16}	1.06	0.75	7.54	0.853	1.01	3.95

- For deep turbulence the Isoplanatic Patch size is many times λ/D
- In addition, the Rytov Number is very much greater than unity

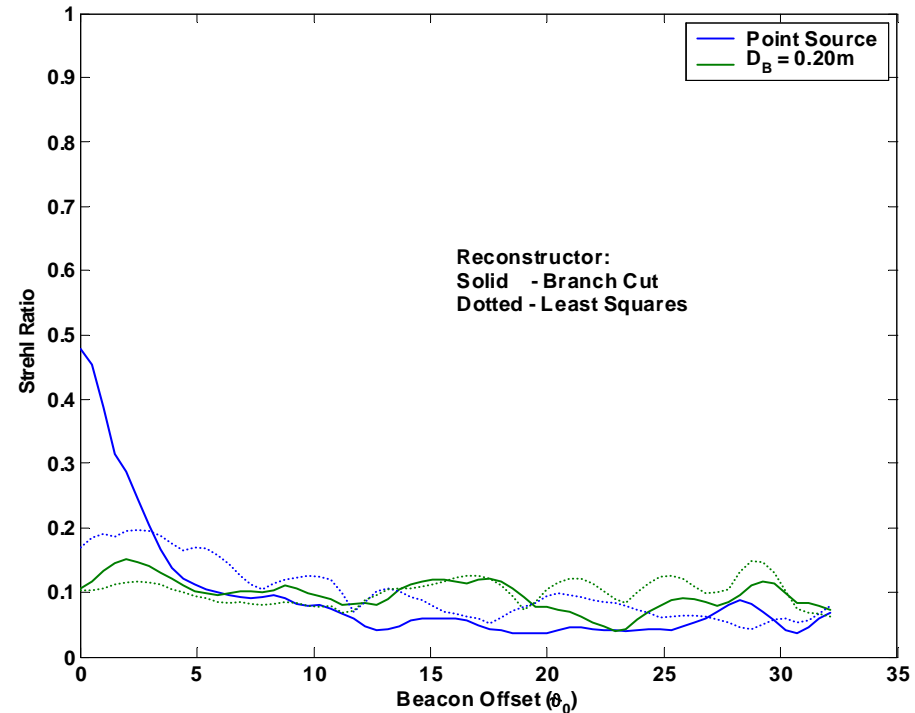
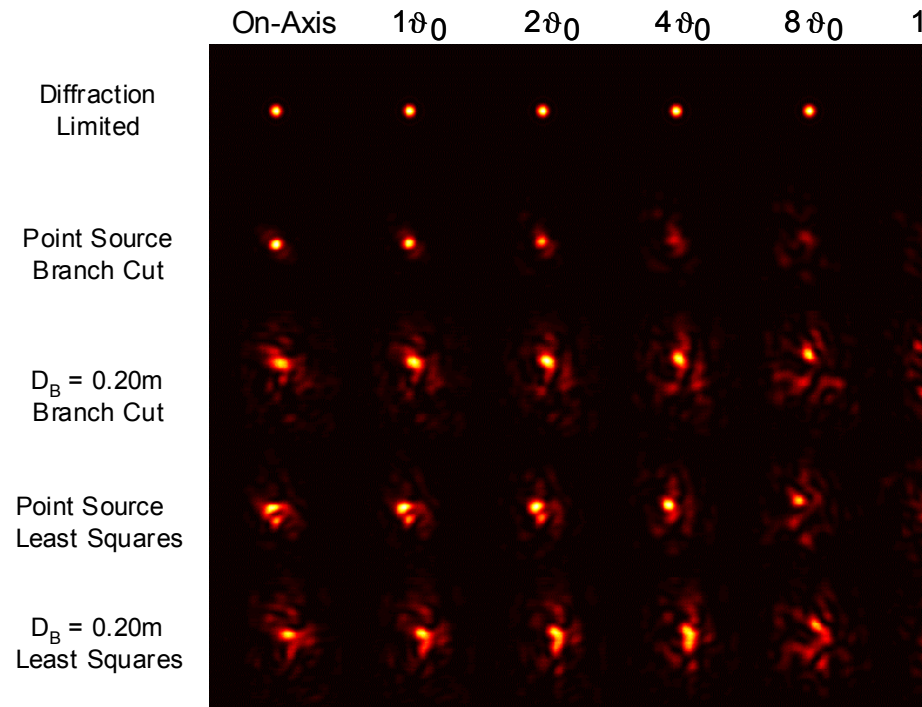
Point and Extended Beacon Irradiance at the Aperture



Anisoplanatism and Finite Beacon Effects upon Perfect AO Compensation



Limitations of Branch Cut Reconstructors in Deep Turbulence



Analysis Summary of Zernike Tomography

- The approach determines the phase correction on N DMs for N beams
- For the case of two beams this requires the solution of two equations and two unknowns

$$\Phi_1(q_{11}\mathbf{r} + l_1\boldsymbol{\vartheta}_1) + \Phi_2(q_{21}\mathbf{r} + l_2\boldsymbol{\vartheta}_1) = -\varphi_1(\mathbf{r}) \quad , \quad q_{ij} = 1 - \frac{l_i}{L_j}$$

$$\Phi_1(q_{12}\mathbf{r} + l_1\boldsymbol{\vartheta}_2) + \Phi_2(q_{22}\mathbf{r} + l_2\boldsymbol{\vartheta}_2) = -\varphi_2(\mathbf{r})$$

- The DM commands, the aberrations and shifted Zernikes are expanded in terms of Zernike polynomials

$$\varphi_n(\mathbf{r}) = \sum_m a_m^{(n)} Z_m\left(\frac{\mathbf{r}}{R}\right) \quad , \quad Z_m\left(\frac{q_{nj}\mathbf{r} + l_n\boldsymbol{\vartheta}_j}{R_n}\right) = \sum_p B_{mp}^{(nj)} Z_p\left(\frac{\mathbf{r}}{R}\right)$$

$$\Phi_n(q_{nj}\mathbf{r} + l_n\boldsymbol{\vartheta}_i) = \sum_m c_m^{(n)} Z_m\left(\frac{q_{nj}\mathbf{r} + l_n\boldsymbol{\vartheta}_j}{R_n}\right) = \sum_m \sum_p c_m^{(n)} B_{mp}^{(nj)} Z_p\left(\frac{\mathbf{r}}{R}\right)$$

- This results in the following expressions

$$\sum_m \sum_p \left[c_m^{(1)} B_{mp}^{(1,1)} + c_m^{(2)} B_{mp}^{(2,1)} \right] Z_p\left(\frac{\mathbf{r}}{R}\right) = \sum_m a_m^{(1)} Z_m\left(\frac{\mathbf{r}}{R}\right)$$

$$\sum_m \sum_p \left[c_m^{(1)} B_{mp}^{(1,2)} + c_m^{(2)} B_{mp}^{(2,2)} \right] Z_p\left(\frac{\mathbf{r}}{R}\right) = \sum_m a_m^{(2)} Z_m\left(\frac{\mathbf{r}}{R}\right)$$

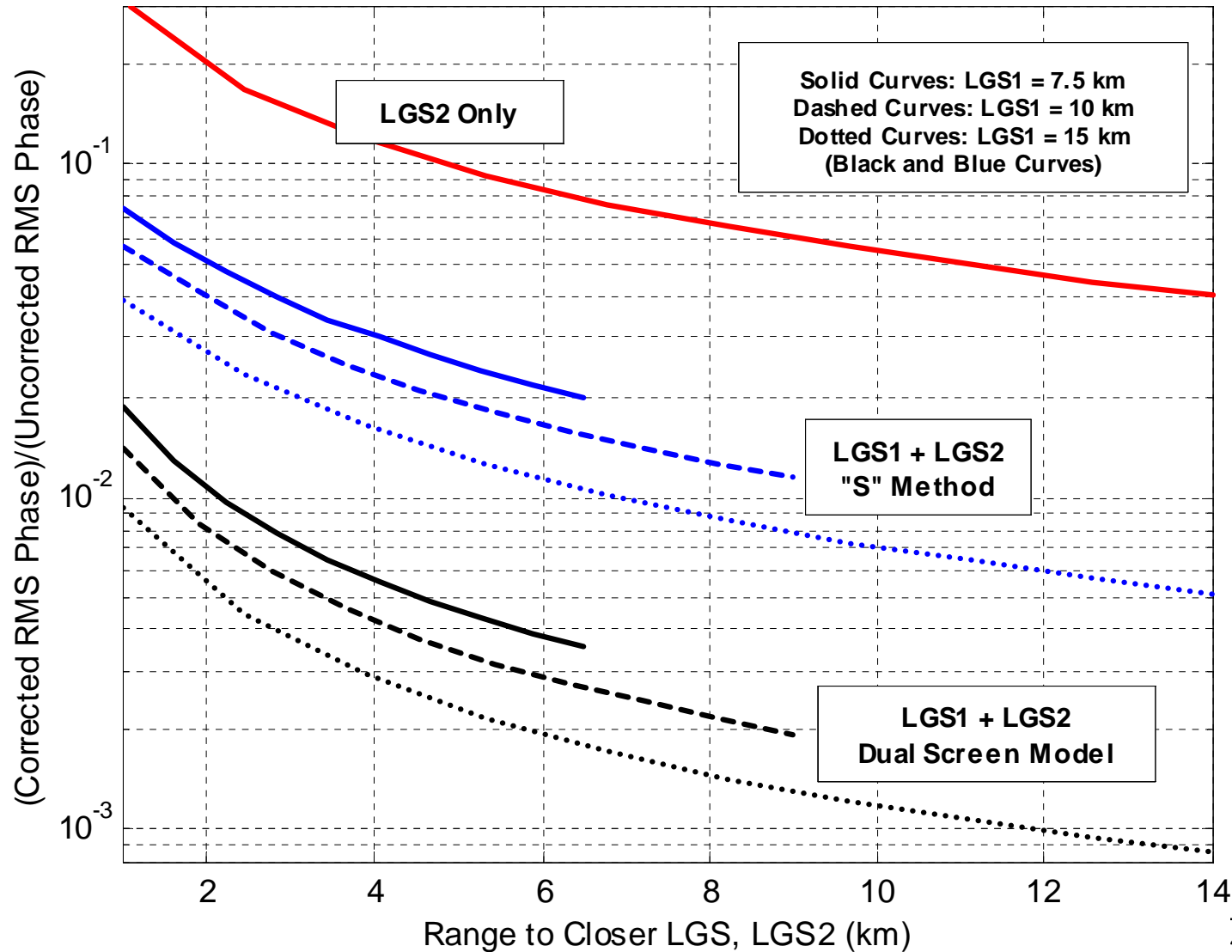
- The DM commands are found by solving the following matrix equation

$$Bc = a$$

Zernike Tomography Performance with Point Source Reference in Weak Turbulence

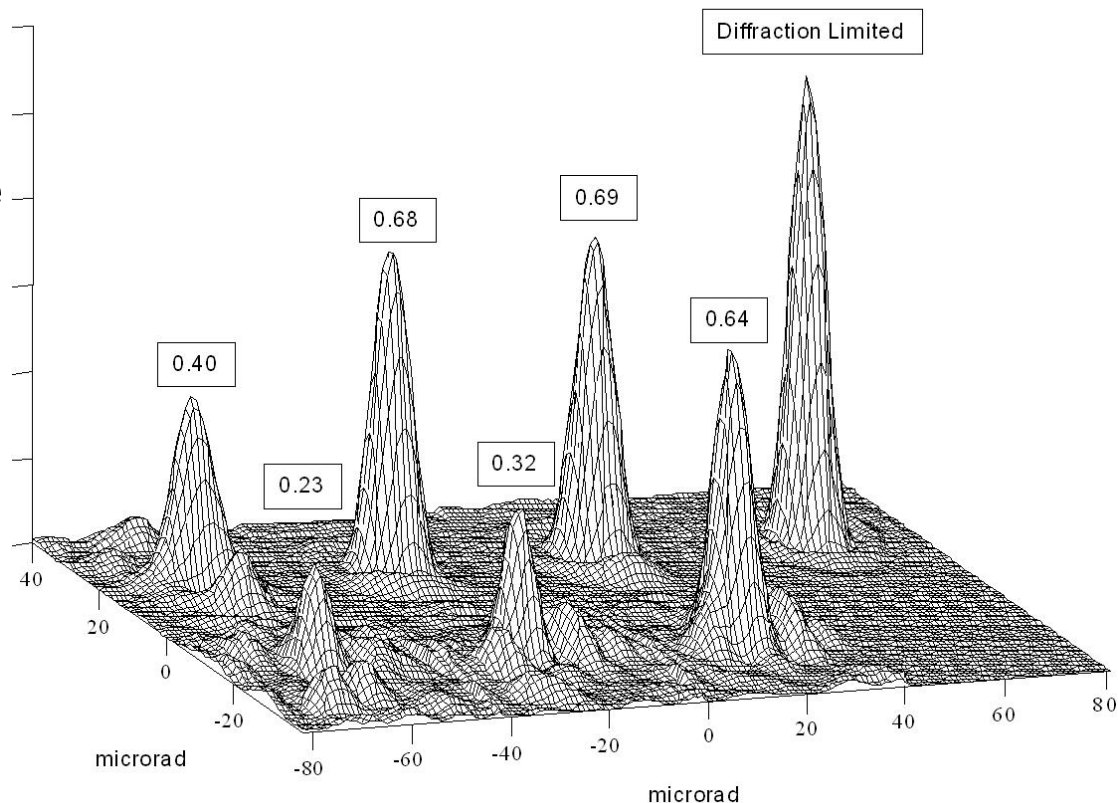
DM Location			ϑ_0 Improvement Factor	Strehl at $10 \vartheta_0$
1	2	3		
0	NONE	NONE	1	6.95×10^{-21}
0.196 L	0.804 L	NONE	6.5	0.129
0.120 L	0.500 L	0.880 L	10.7	0.409

Initial Comparison of Near Field Compensation Approaches

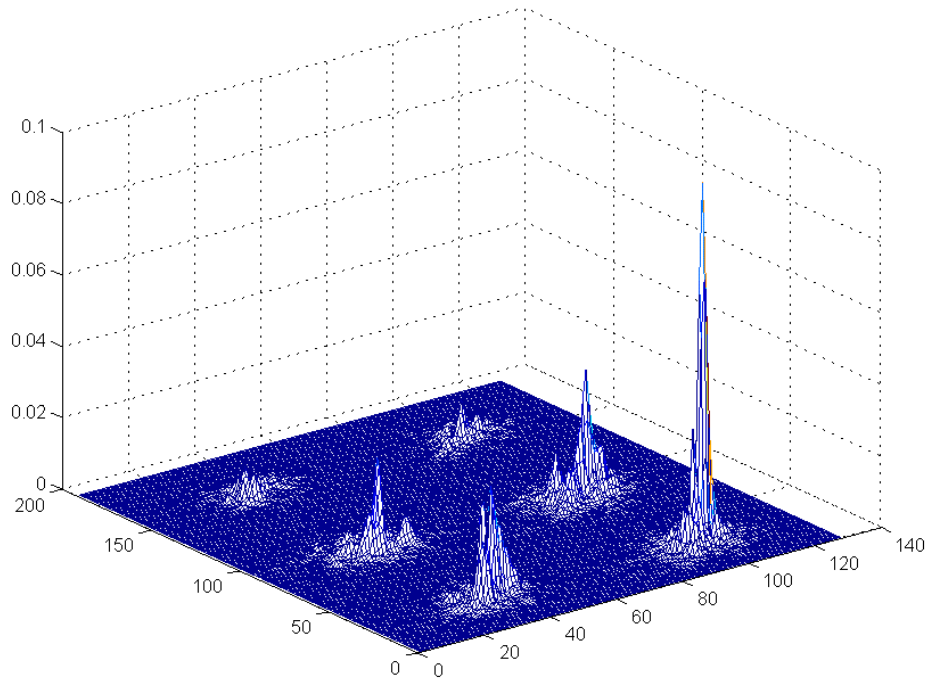


Gradient Descent Tomography in Weak Turbulence

- Gradient Descent Tomography is implemented by using an image based merit function
- In the work here we dither the actuators on one or two deformable mirrors and use a gradient search technique to optimize the integral I^2 image sharpening merit function
- The results on the right illustrate that Anisoplanatism is significantly reduced when the MCAO 2 DM version of this approach is utilized
- The use of only one DM corrects only one field angle



Performance of Gradient Descent Tomography in Deep Turbulence



Strehl Ratio Computed from a Wave Optics Simulation			
Object	Uncompensated Strehl	Compensated Strehl	PIR
Point #1	0.0081	0.0097	1.20
Point #2	0.0252	0.0337	1.34
Point #3	0.0304	0.0992	3.26

Conclusions

- Interesting approaches have been developed for adaptive optics compensation of a laser transmitter or an imaging system for propagation through strong turbulence
 - Branch cut reconstructors
 - MCAO concepts
- Analysis tools are mature
 - Fast least squares
 - Perturbation theory
- Experimental tests of promising approaches are being considered
- Results impact
 - Low elevation astronomy
 - Laser communications
 - Power beaming (relay mirrors)
 - Compensation through deep turbulence